Structural Interpretation of RADARSAT-1 Principal Components Imagery and Its Potential Application to Kimberlite Exploration in the Buffalo Head Hills Area, North Central Alberta

104-03616/

Structural Interpretation of RADARSAT-1 Principal Components Imagery and Its Potential Application to Kimberlite Exploration in the Buffalo Head Hills Area, North Central Alberta

F. Paganelli[1], E.C. Grunsky[2] and J.P. Richards[1]

[1]Department of Earth & Atmospheric Sciences, University of Alberta

[2]Alberta Geological Survey

July 2003

©Alberta Energy and Utilities Board, 2003

The Alberta Energy and Utilities Board/Alberta Geological Survey (EUB/AGS) and its employees and contractors make no warranty, guarantee or representation, express or implied, or assume any legal liability regarding the correctness, accuracy, completeness or reliability of this publication. Any digital data and software supplied with this publication are subject to the licence conditions. The data are supplied on the understanding that they are for the sole use of the licensee, and will not be redistributed in any form, in whole or in part, to third parties. Any references to proprietary software in the documentation and/or any use of proprietary data formats in this release do not constitute endorsement by the EUB/AGS of any manufacturer's product.

If this product is an EUB/AGS Special Report, the information is provided as received from the author and has not been edited for conformity to EUB/AGS standards.

When using information from this publication in other publications or presentations, due acknowledgment should be given to the EUB/AGS. The following reference format is recommended:

Paganelli, F., Grunsky, E.C and Richards, J.P. (2002): Structural interpretation of RADARSAT-1 principal components imagery and its potential application to kimberlite exploration in the Buffalo Head Hills area, north central Alberta; Alberta Energy and Utilities Board, EUB/AGS Special Report 21.

Published July 2003 by:
Alberta Energy and Utilities Board
Alberta Geological Survey
4th Floor, Twin Atria Building
4999 – 98th Avenue
Edmonton, Alberta
T6B 2X3

Tel: (780) 422-3767 (Information Sales)
Fax: (780) 422-1918
E-mail: EUB.AGS-Infosales @gov.ab.ca

Web site: www.ags.gov.ab.ca

Contents

Acknowledgements v
Abstract vi
1 Introduction 1
1.1 RADARSAT-1 Data Acquisition, Pre-Processing and Mosaicing 2
1.2 RADARSAT-1 Data 2
1.3 RADARSAT-1 Pre-Processing 4
1.4 RADARSAT-1 Mosaicing 4
2 Principal Components Analysis of RADARSAT-1 Imagery 4
2.1 RADARSAT-1 Statistical Processing 14
2.2 RADARSAT-1 Principal Component Imagery 16
2.3 Statistics of RADARSAT-1 PC Imagery 16
3 Structural Interpretation of RADARSAT-1 Principal Component Images 22
3.1 RADARSAT-1 PC Structural Interpretation 24
3.2 RADARSAT-1 PC1 Structural Interpretation 24
3.3 RADARSAT-1 PC2 Structural Interpretation 38
3.4 RADARSAT-1 PC3 Structural Interpretation 39
3.5 RADARSAT-1 PC4 Structural Interpretation 40
4 Tectonic Framework 40
4.1 North-Northeast?Trending Lineaments 40
4.2 Northwest-Trending Lineaments 40
4.3 Northeast-Trending Lineaments 41
4.4 East-Northeast?Trending Lineaments 41
4.5 Discussion of the Outlined Structural Trends 41
5 Preliminary Integration of RADARSAT-1 Principal Components, Digital Elevation Data, Geological Structure and Kimberlite Locations 43
5.1 RADARSAT-1 PC Colour Composite Imagery, Structural Data and Kimberlite Locations 43
5.2 RADARSAT-1 PC123 (RGB) 43
5.3 RADARSAT-1 PC Colour Composite, DEM, Structural Data and Kimberlite Locations 43
5.4 RADARSAT-1 PC, Geology, Structural Data and Kimberlite Locations 46
6 Considerations for Further Work 46
7 References 48
Appendix 1 – RADARSAT-1 Scene ID and Acquisition Date 50
Appendix 2 – RADARSAT-1 Filtered Scenes 51
Appendix 3 – RADARSAT-1 Mosaic Scenes 52

Tables

Table 1 RADARSAT-1 multi-band image MOSAIC_S1-S7 PCA statistics 14
Table 2 RADARSAT-1 PC multi-band image PC_MOSAIC_S1-S7 statistics 22

Figures

Figure 1 Buffalo Head Hills study area and NTS coverage 1
Figure 2 Buffalo Head Hills geology and kimberlite occurrences 3
Figure 3 Coverage RADARSAT-1 S1 Ascending Mode 5

Figure 4 Coverage RADARSAT-1 S1 Descending Mode 6
Figure 5 Coverage RADARSAT-1 S7 Ascending Mode 7
Figure 6 Coverage RADARSAT-1 S7 Descending Mode 8
Figure 7 Intersection coverage of RADARSAT-1 multi-beam S1/S7 Ascending/Descending Mode imagery 9
Figure 8 Mosaic of 8 filtered RADARSAT-1 S1 Ascending scenes 10
Figure 9 Mosaic of 8 filtered RADARSAT-1 S1 Descending scenes 11
Figure 10 Mosaic of 6 filtered RADARSAT-1 S7 Ascending scenes 12
Figure 11 Mosaic of 6 filtered RADARSAT-1 S7 Descending scenes 13
Figure 12 Scattergrams of multi-beam RADARSAT-1 S1/S7 Ascending/Descending imagery 15
Figure 13 Mosaic coverage and intersection of S1-S7 ascending and descending RADARSAT-1 imagery 17
Figure 14 First Principal Component (PC1) from multi-beam RADARSAT-1 imagery. 18
Figure 15 Second Principal Component (PC2) from multi-beam RADARSAT-1 imagery 19
Figure 16 Third Principal Component (PC3) from multi-beam RADARSAT-1 imagery 20
Figure 17 Fourth Principal Component (PC4) from multi-beam RADARSAT-1 imagery 21
Figure 18 Scattergrams of principal components derived from multi-beam RADARSAT-1 S1/S7 Ascending/Descending imagery 23
Figure 19 Geology of the Buffalo Head Hills over the second principal component (PC2) 25
Figure 20 Principal Component1 (PC1) with structural interpretation derived from PC1 26
Figure 21 Principal Component 2 (PC2) with structural interpretation derived from PC2 27
Figure 22 Principal Component 3 (PC3) with structural interpretation derived from PC3 28
Figure 23 Principal Component 4 (PC4) with structural interpretation derived from PC4 29
Figure 24 Principal Component 2 (PC2) with N-NE lineament compilation 30
Figure 25 Principal Component 2 (PC2) with NW lineament compilation 31
Figure 26 Principal Component 2 (PC2) with NE lineament compilation 32
Figure 27 Principal Component 2 (PC2) with ENE lineament compilation 33
Figure 28 Colour composite Principal Components 1 (red), 2 (green) and 3 (blue) with structural trends and kimberlite locations 44
Figure 29 Colour composite Principal Components 1 (red), 2 (green) and 3 (blue) draped on a Digital Elevation Model (DEM) with structural trends and kimberlite locations 45
Figure 30 Geology of the Buffalo Head Hills draped on RADARSAT-1 PC2 with structural trends and kimberlite locations 47

Maps

1 Principal Component 2 (PC2) with N-NE lineament compilation 34
2 Principal Component 2 (PC2) with NW lineament compilation 35
3 Principal Component 2 (PC2) with NE lineament compilation 36
4 Principal Component 2 (PC2) with ENE lineament compilation 37

Acknowledgements

The data used in this study were provided through the Provincial Partnership Memorandum Of Understanding agreement between the Province of Alberta and the Canadian Space Agency. The authors wish to acknowledge the opportunity to acquire and use the data for the purposes of demonstrating applications for RADARSAT-1 satellite imagery.

The authors are grateful for the assistance of Ken Dutchak and Bob Sleep of the Resource Data Division of Alberta Sustainable Development (Edmonton).

The Resource Data Division and the Alberta Geological Survey provided the necessary funding that enabled the acquisition of the RADARSAT-1 imagery.

This work was carried out as a preliminary study to provide data availability and access for a Ph.D. project at the University of Alberta. Support was provided by Alberta Geological Survey and the University of Alberta.

Abstract

Principal components analysis (PCA) of RADARSAT-1 satellite imagery has been used to enhance the interpretation of surface features that may reflect underlying bedrock structures. Application of this technique in the Buffalo Head Hills area of north central Alberta, a region of active kimberlite exploration, suggests that the results may provide an indication of deeper crustal structures that controlled the emplacement of kimberlite intrusions. The method may, therefore, provide an important first-pass tool for exploration.

Four RADARSAT-1 principal components (RADARSAT-1 PCs) were extracted from RADARSAT-1 Standard Beam Mode S1 and S7 scenes, acquired in ascending and descending modes of the satellite's orbit (i.e., flying south to north and vice versa). A structural analysis of the principal component images provided sufficient detail to outline the major lineaments characterizing the meso- and mega-scale structures of the Buffalo Head Hills. The use of the PCA method minimizes data redundancy inherent in the RADARSAT-1 images and emphasizes the unique information contained in each scene as a response to the radar backscattering to surface roughness, surface dielectric properties, slope attitude and vegetation canopy variations.

North- and north-northeast-trending lineaments that bound the eastern edge of the Buffalo Head Hills along the Loon River graben (Eccles et al., 2000) were delineated. A conjugate set of northwest and northeast-trending lineaments that form block fault structures within the Buffalo Head Hills and along the eastern boundary have been outlined. East-northeast trending lineaments have been identified as the latest event in the area that offset the north-, north-northeast-, and northwest-trending structures. These structures extend throughout the Buffalo Head Hills and Loon River graben.

Integration of RADARSAT-1 PC images and digital elevation models (DEM) of the surface topography and Precambrian basement have been used to extract key structural and morphological features, which have then been compared with the locations of known kimberlites reported in Eccles et al. (2000). Interpreted surface intersections of north-northeast-, northwest and east-northeast–trending lineaments show first-order spatial correlations with these kimberlite occurrences. The youngest east-northeast-trending lineaments are thought to be of middle to upper Cretaceous age and may, therefore, have influenced the locations of kimberlite emplacement, which is believed to have occurred during the Upper Cretaceous.

1 Introduction

The Buffalo Head Hills area extends north of the east-northeast–trending Peace River Arch, which affected the Phanerozoic succession of sediments in the Western Canada Sedimentary Basin (WCSB) (Figure 1). The Buffalo Head Hills is part of the cratonic platform whose tectonic evolution has been influenced by the uplift and extensional episodes of the Peace River Arch (Cant, 1988; O'Connell et al., 1990), with the Phanerozoic development of north-trending horst-graben block structures. The Buffalo Head Hills is characterized by a sedimentary succession of platform carbonates, shale and sandstone of Devonian and Cretaceous ages, overlying the Precambrian crystalline metamorphic basement (Edwards et al., 1995). The Precambrian basement is here defined by the Buffalo Head High (BH) and Buffalo Head Utikuma (BU) terranes, whose differentiation is based on the distinct magnetic high response of the BH and magnetic variable response from high to low of the BU (Pilkington et al., 2000).

Figure 1. Buffalo Head Hills study area and NTS coverage.

A previous remote sensing study, which was conducted in the Peerless Lake area (Eccles et al., 2000), included the southeast corner of the Buffalo Head Hills and encompassed several kimberlite occurrences. The kimberlite pipes occur along the eastern flank of the Buffalo Head Hills, parallel to the Loon River Lowlands, and occur near or at the intersection of north- and northeast-trending lineaments. Preliminary petrographic examination of the kimberlites indicates they consist of pyroclastic crater facies, mainly of lapilli-bearing, olivine-rich crystal tuffs. Crustal xenoliths are typically shales of the Shaftesbury Formation (Lower Cretaceous), whereas mantle-derived xenoliths include peridotitic, pyroxenitic, eclogitic and corundum-spinel-bearing lithologies. Uranium-Lead (U-Pb) perovskite dates of 86+3 and 88+5 Ma (Carlson et al., 1998) suggest that the pipes were emplaced within the WCSB, in sediments of the Mid to Late Cretaceous (Cenomanian to Campanian) Smoky Group, Dunvegan Formation and possibly Shaftesbury Formation (Figure 2).

Little is known of the geology of the Buffalo Head Hills area, and although remotely sensed data, including high resolution aeromagnetics and seismic surveys, have been used by the oil and gas industry to the west over the Peace River Arch, these results remain in the private domain.

Principal components analysis (PCA) of RADARSAT-1 images (Grunsky, 2002) obtained over the Buffalo Head Hills area of northern central Alberta (Figure 1) has been tested for its utility in structural mapping, with specific application for kimberlite exploration. The geology and digital elevation models (DEM) of surface and Precambrian basement topography have been integrated with the RADARSAT-1 PC2 (second principal component) image to outline structural features correlation with surface and basement characteristics, which has then been compared with the locations of known kimberlite occurrences in the area.

The data used in this study have been provided by the Alberta Geological Survey (AGS) and constitutes material from a comprehensive exploration project in north central Alberta. Image processing software (ERMapper version 6.1) has been used for image integration and map compilation.

1.1 RADARSAT-1 Data Acquisition, Pre-Processing and Mosaicing

The use of radar imagery has been commonly employed for mapping geomorphology and geological structure (Gupta, 1991; Singhroy and Saint-Jean, 1999; Smith et. al., 1999). The range of incidence angles, all-weather atmospheric penetration and response to surface morphology are significant advantages for mapping geomorphology and surface structure.

RADARSAT-1 satellite imagery has been evaluated for its potential to provide useful, regional-scale information for geological mapping and as an aid to structural mapping in both barren and highly vegetated terrains throughout Canada (Singhroy et al., 1993; Berger and Cartwright, 1997; Paganelli and Rivard, 2001).

Details on the characteristics of RADARSAT-1 satellite images, including a description of beam modes, resolutions and coverage can be found in the Radarsat Users Guide (Radarsat International, 1999) and Radarsat Geology Handbook (Radarsat International, 1996).

1.2 RADARSAT-1 Data

A total of 28 RADARSAT-1 scenes in Standard Beam S1 and S7 modes (12.5 m pixel resolution), which were obtained during ascending and descending satellite orbits, were acquired to provide full coverage

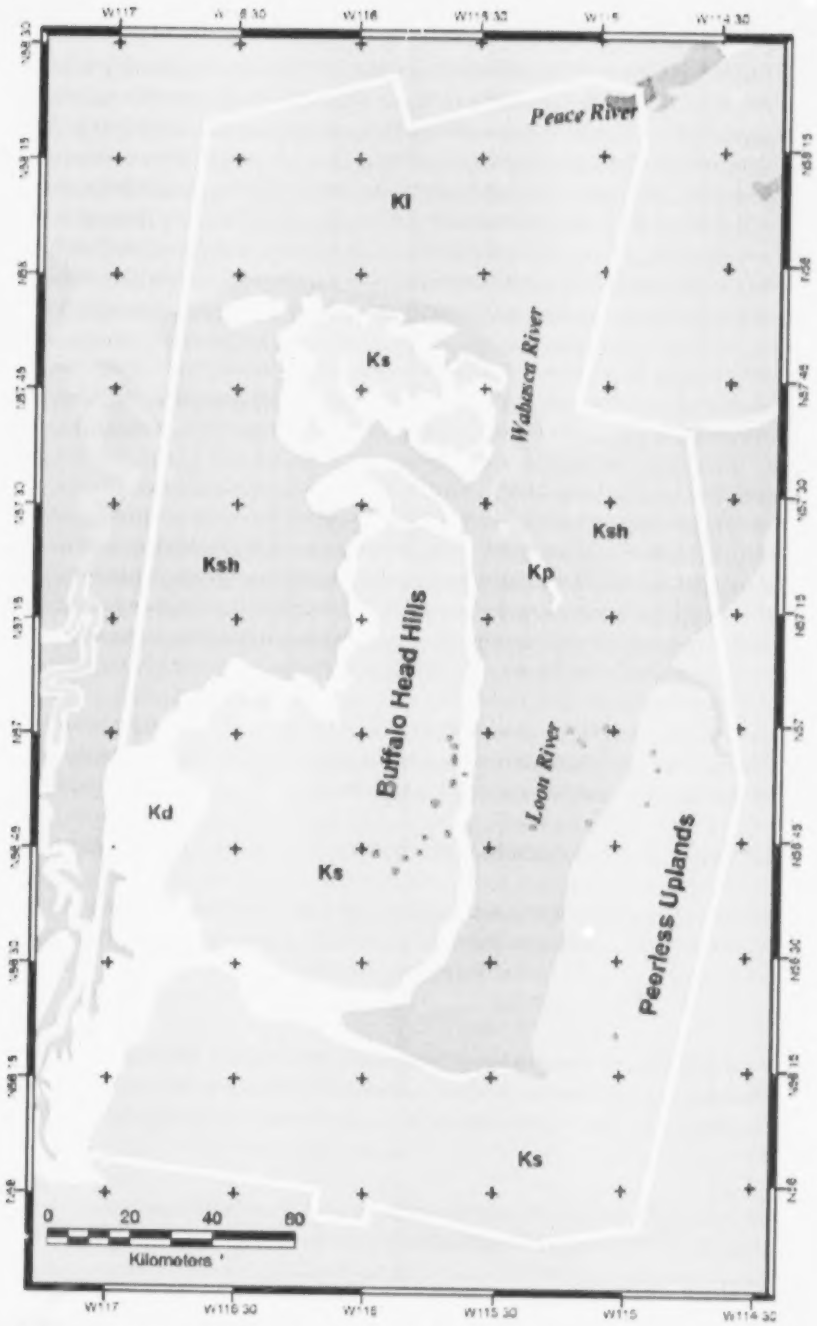

Figure 2. Buffalo Head Hills geology and kimberlite occurrences (red): Kl, Loon River Formation (Lower Cretaceous); Kp, Peace River Formation (Lower Cretaceous); Ksh, Shaftesbury Formation (Lower-Upper Cretaceous); Kd, Dunvegan Formation (Upper Cretaceous); Ks, Smoky Group (Upper Cretaceous); kimberlite, red circle. Study area outlined in white.

of the Buffalo Head Hills area. These images are part of a data set of a large-scale project covering northern Alberta (Grunsky, 2001). The images provide four different inherent geometric configurations that combine the different incidence angles of the S1 (20°-27.4°) and S7 (44.9°-49.4°) modes (Luscombe et al., 1993), and different look directions (east or west) depending on the geometry of the acquisition mode in ascending and/or descending orbit. The RADARSAT-1 coverage for each data set is shown in Figures 3 to 6, and the intersection coverage defining the Buffalo Head Hills study area is shown in Figure 7.

The Buffalo Head Hills area defines a moderate topographic high (up to 220 m local relief) characterized by an east-facing slope toward the Loon River valley. Another topographic high is defined by the Peerless Uplands, which have a westward-facing slope toward the Loon River Valley. Both the Buffalo Head Hills and Peerless Uplands define north-trending topographic features whose contrast can be either emphasized or suppressed in the different orbit mode images. An optimal geometric configuration to highlight this major topographic trend is provided by the RADARSAT-1 S1 and S7 descending images, which are characterized by east to west look directions (Figures 8 and 9). An opposite effect is given by the RADARSAT-1 S1 and S7 ascending images because they are characterized by an opposite look direction from west to east (Figures 10 and 11). Steeper incidence angles provided in the RADARSAT-1 S1 mode emphasize the gentle topography of the area; compare, for example, the sharp contrast visible in MOSAIC_S1D (Figure 8) with the subdued contrast in the MOSAIC_S7D (Figure 9). These geometrical factors induce inherent characteristics in the image that are reflected in the data distribution and, therefore, will affect the input contribution that each mosaic scene will give in the processing of the principal components analysis.

The image dataset has been orthorectified using the UTM projection (Zone 11, NAD83) by RGI Ltd. (Vancouver). A list of the images and their parameters is provided in Appendix 1.

1.3 RADARSAT-1 Pre-Processing

The RADARSAT-1 scenes have been pre-processed for speckle reduction to reduce the inherent "salt and pepper" noise in radar imagery, using an 11x11 Gaussian filter with a standard deviation of 1.6 (Lewis et al., 1998), which corresponds to a smoothing function equivalent to a normal distribution with limits to the 95% of the area under the curve. This process produces smoother images with more uniform tonal characteristics. The list of filtered images is provided in Appendix 2.

1.4 RADARSAT-1 Mosaicing

To conduct the regional investigation of the Buffalo Head Hills area, the RADARSAT-1 filtered scenes have been combined into a mosaic. The mosaicing of the filtered scenes has been conducted using linear stretch matching, smoothing and feather filtering options to smooth the image tonal changes and edges between the individual scenes. Four mosaic scenes have been obtained and used as a source dataset for the PCA. The mosaics are shown in Figures 8 to 11, and the source images are listed in Appendix 3.

2 Principal Components Analysis of RADARSAT-1 Imagery

The method of principal components analysis (Mather, 1982) is performed to reduce data redundancy inherent in the radar imagery and to produce four single-band images that express linear combinations (components) of the data distribution of the original dataset. These images, therefore, emphasize combined characteristics of the source data that are based on the correlation between the input channels.

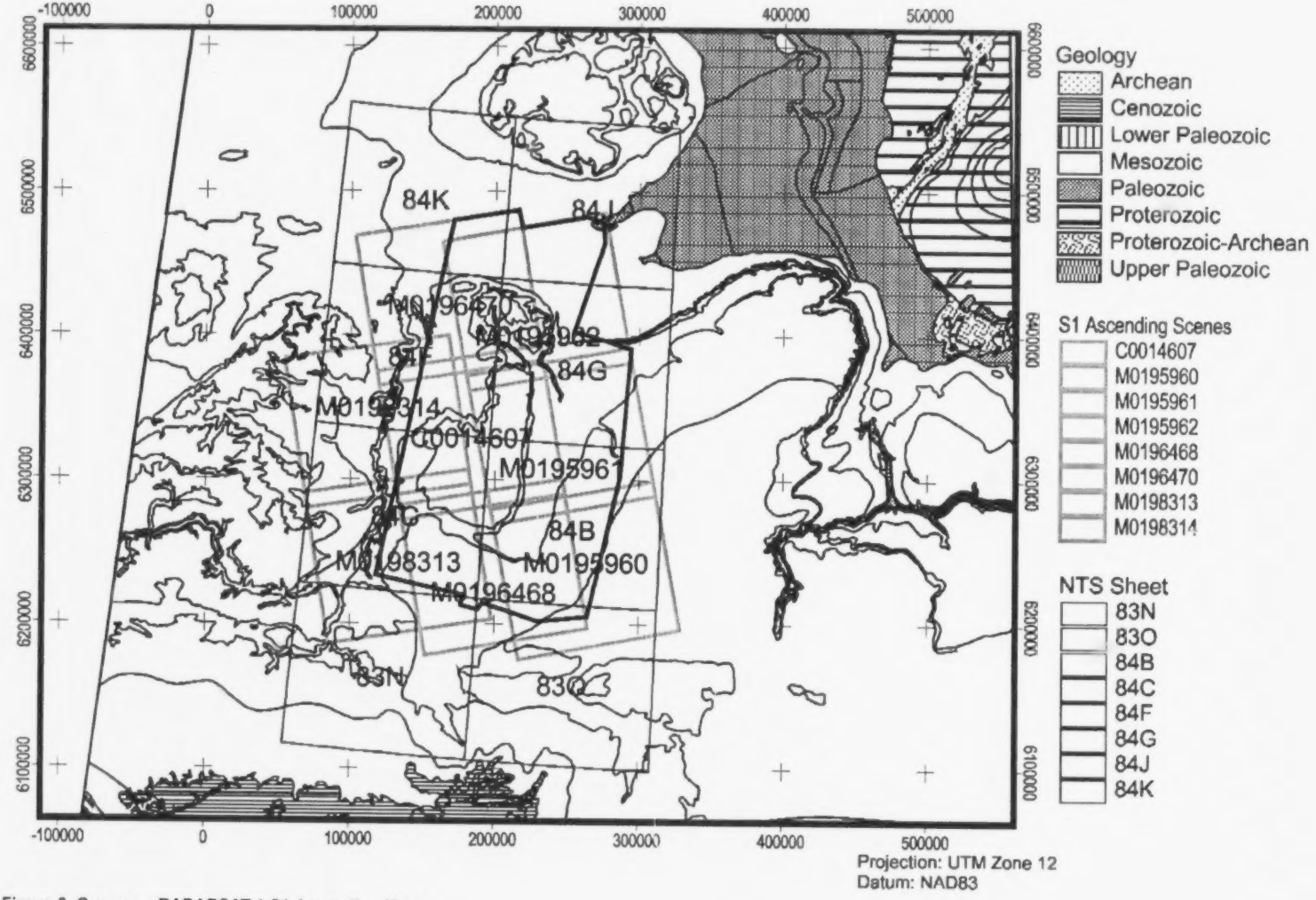

Figure 3. Coverage RADARSAT-1 S1 Ascending Mode.

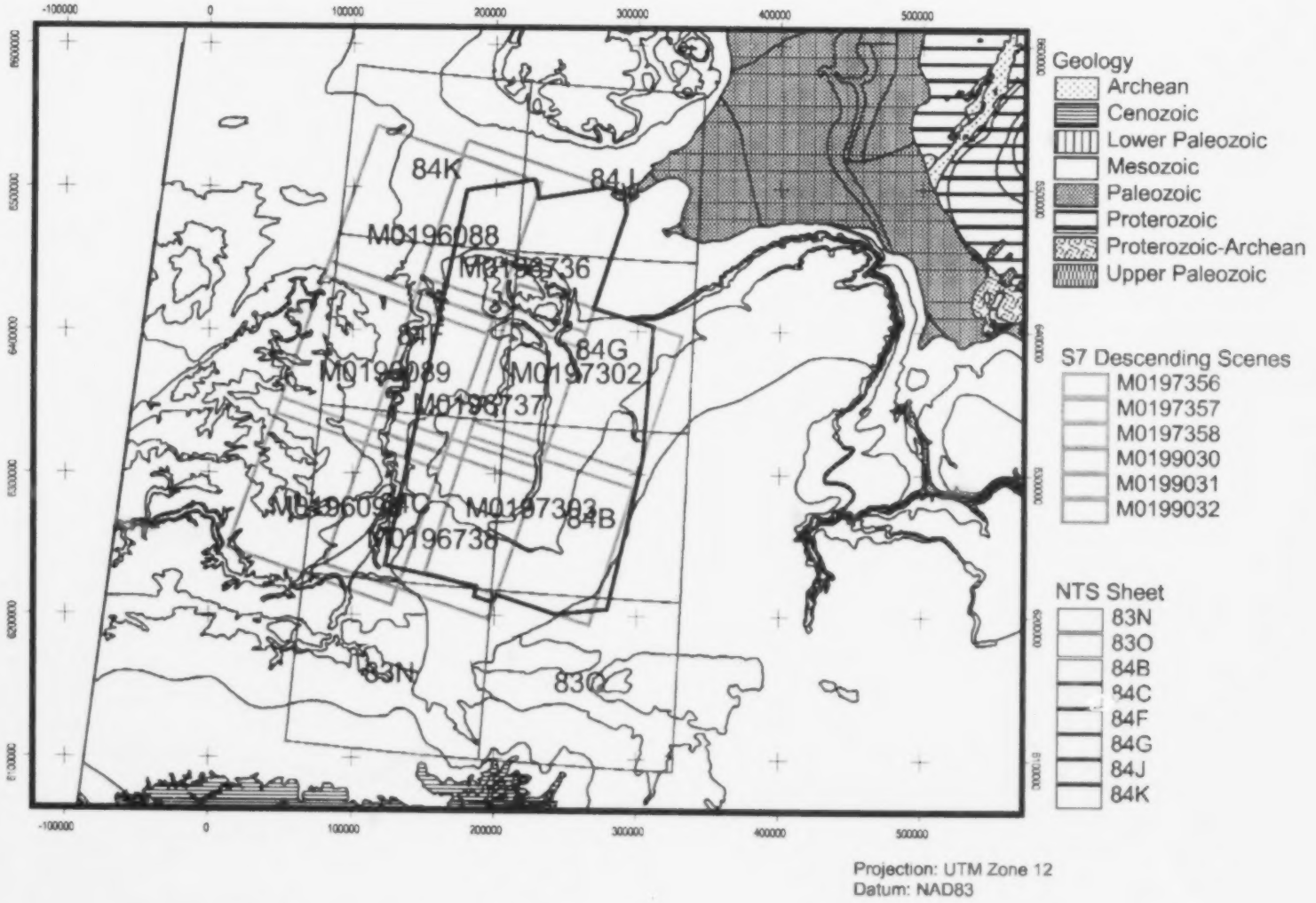

Figure 4. Coverage RADARSAT-1 S1 Descending Mode.

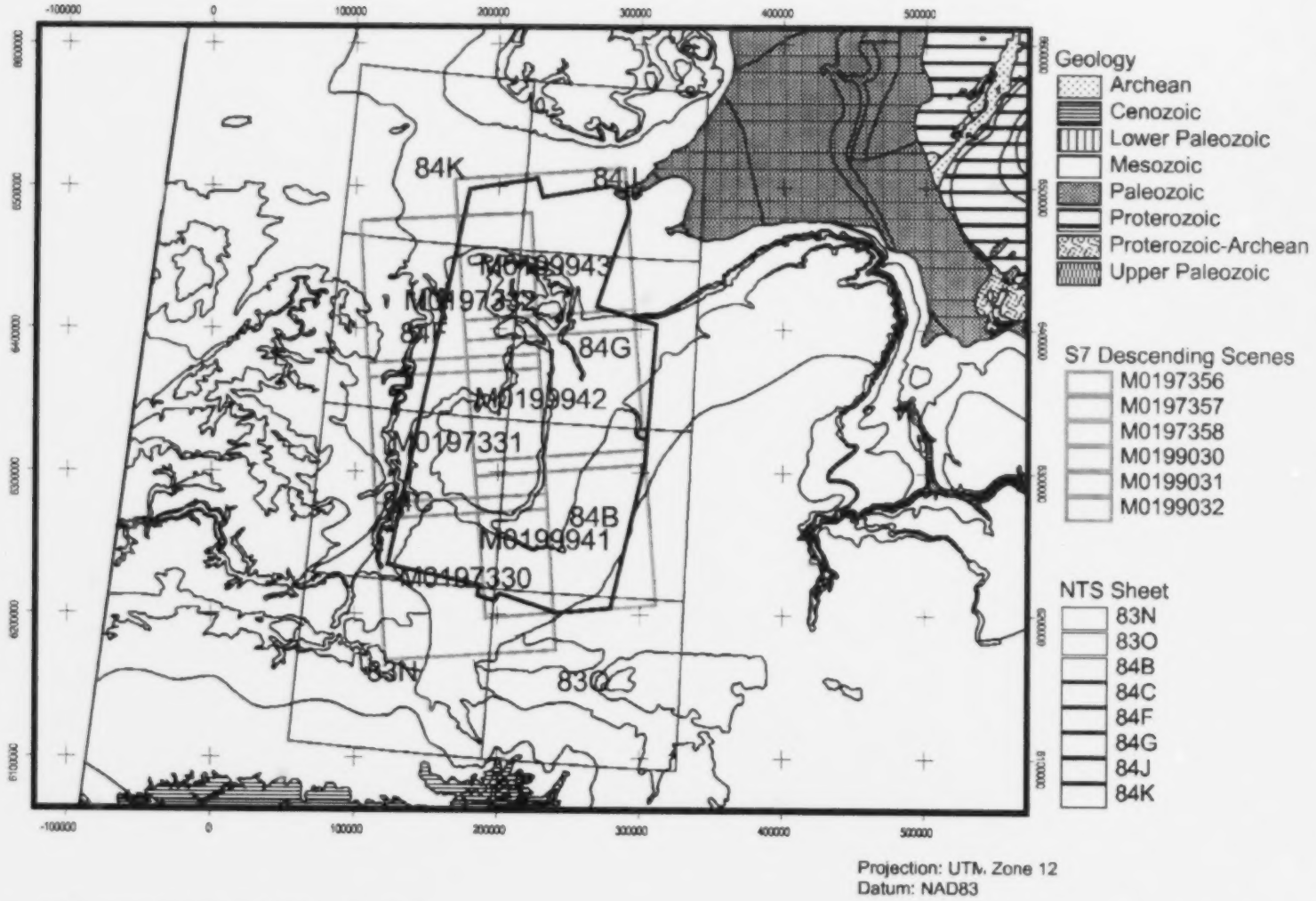

Figure 5. Coverage RADARSAT-1 S7 Ascending Mode.

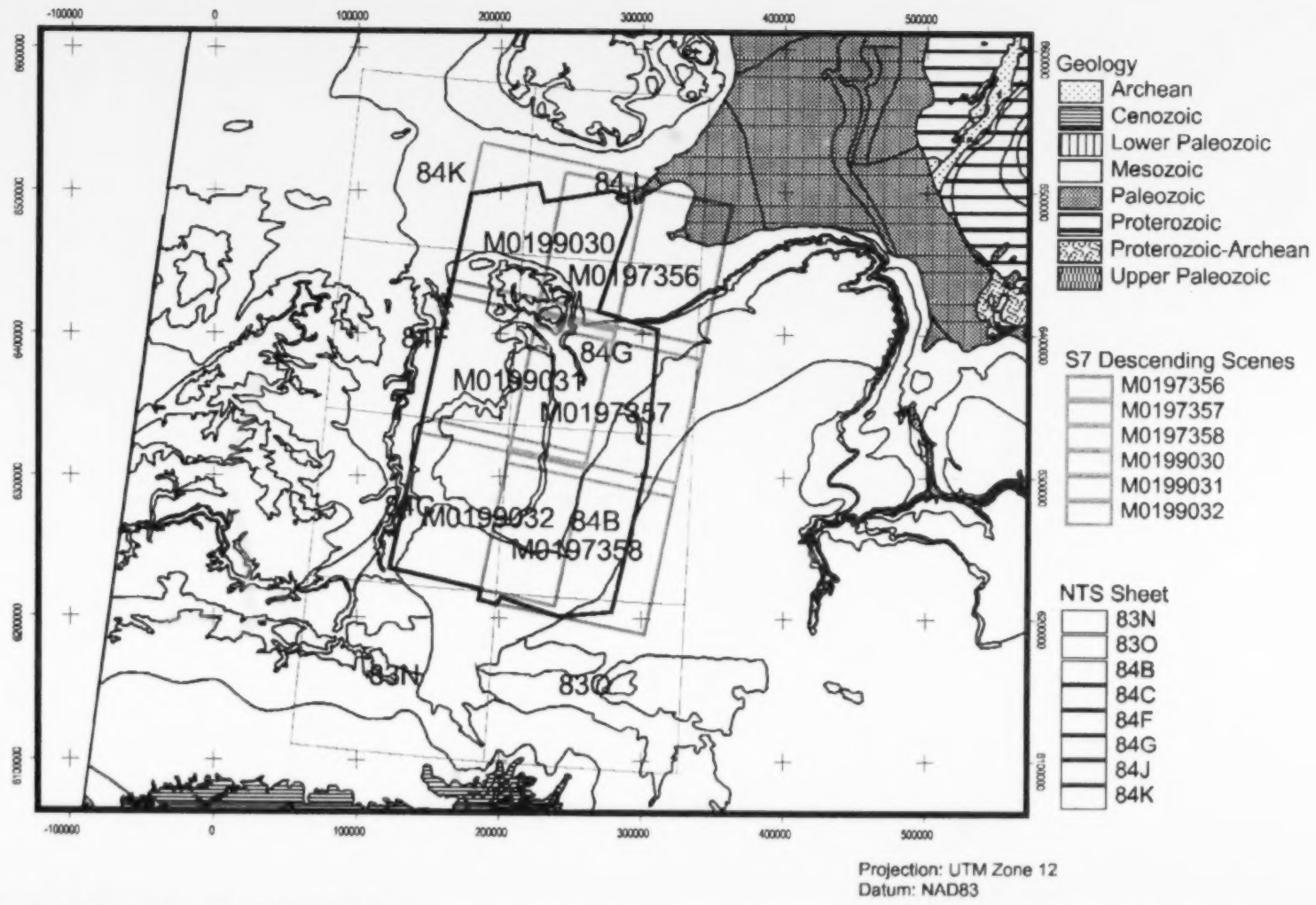

Figure 6. Coverage RADARSAT-1 S7 Descending Mode.

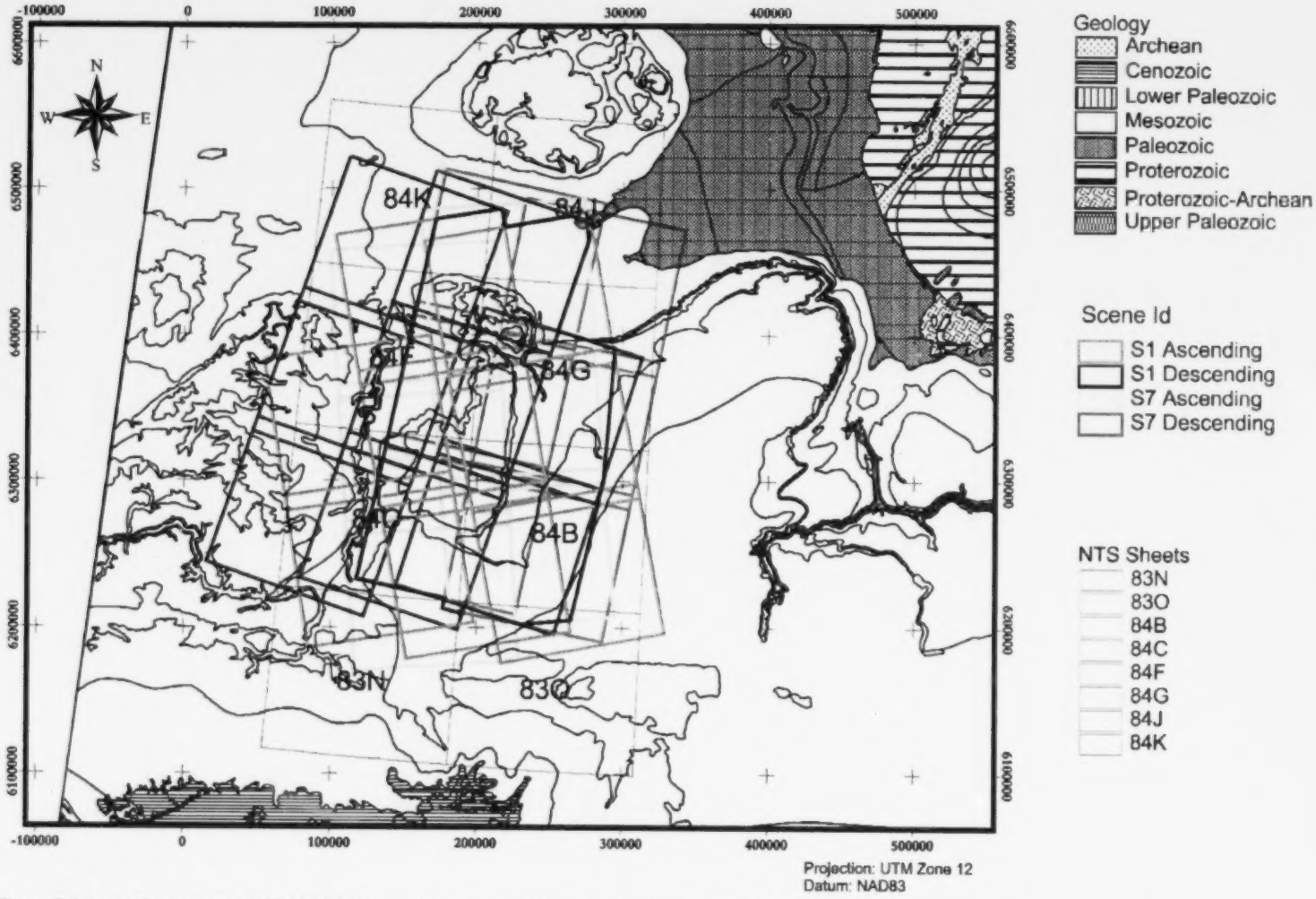

Figure 7. Intersection coverage of RADARSAT-1 multi-beam S1/S7 Ascending/Descending Mode imagery.

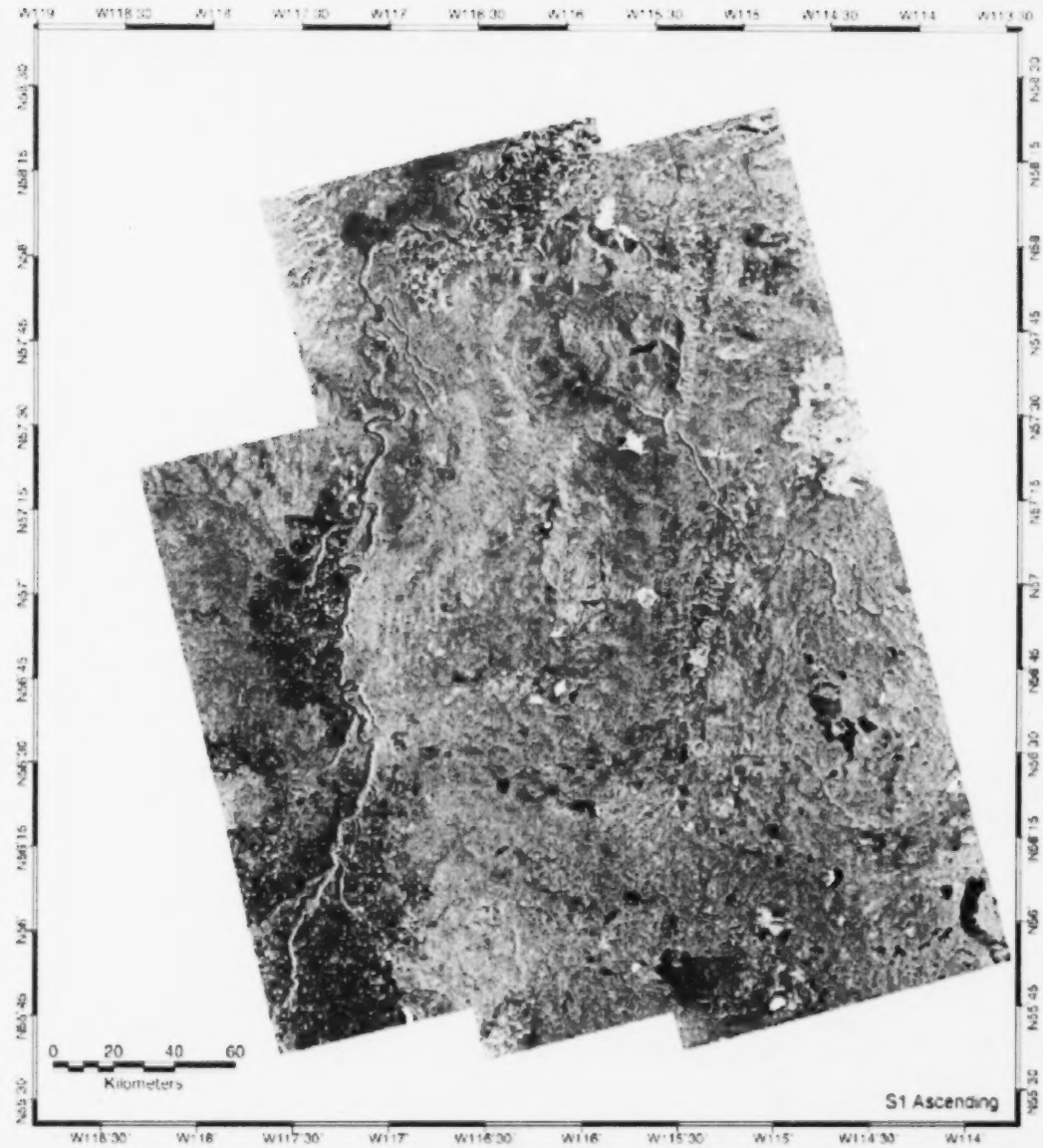

Figure 8. Mosaic of eight filtered RADARSAT-1 S1 Ascending scenes.

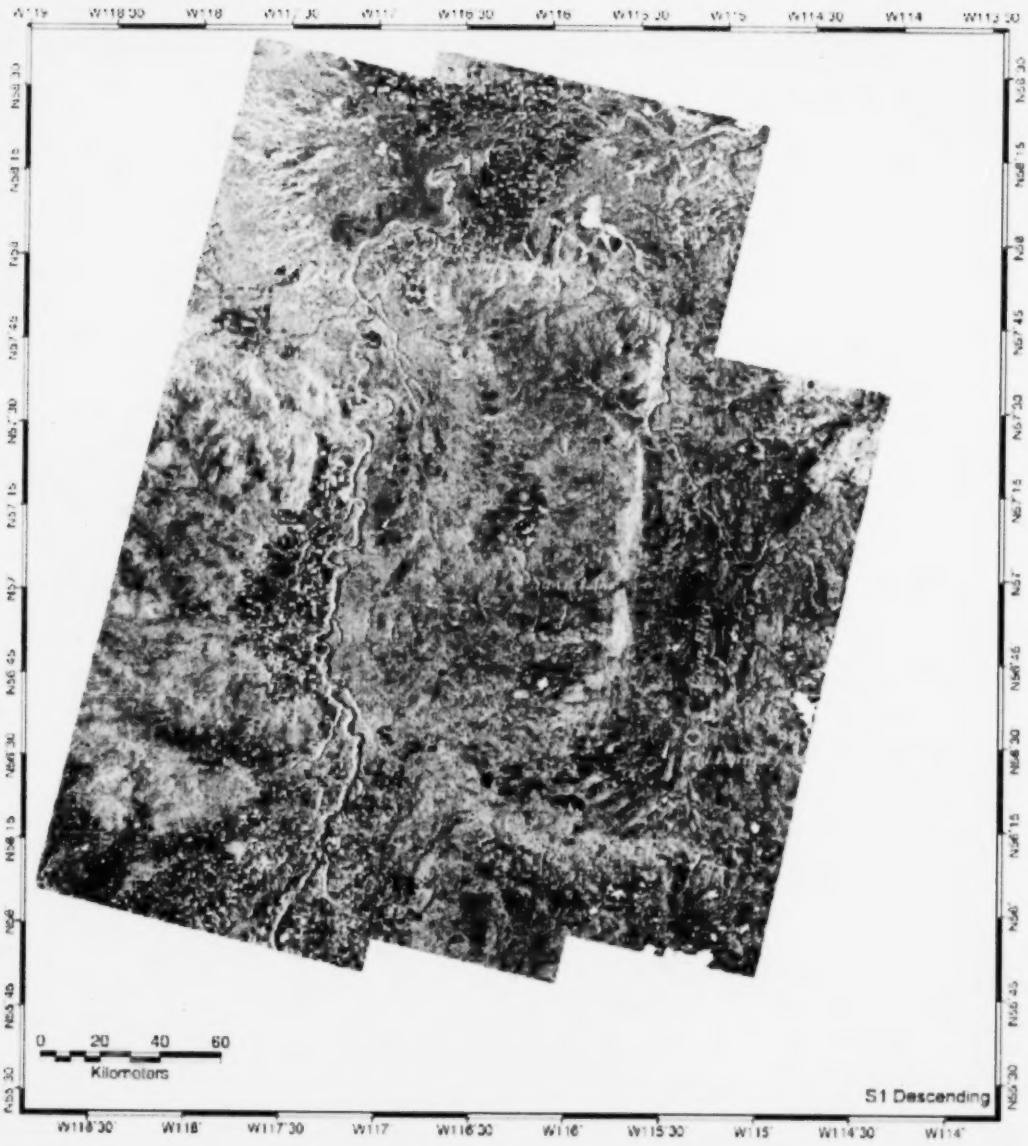

Figure 9. Mosaic of eight filtered RADARSAT-1 S1 Descending scenes.

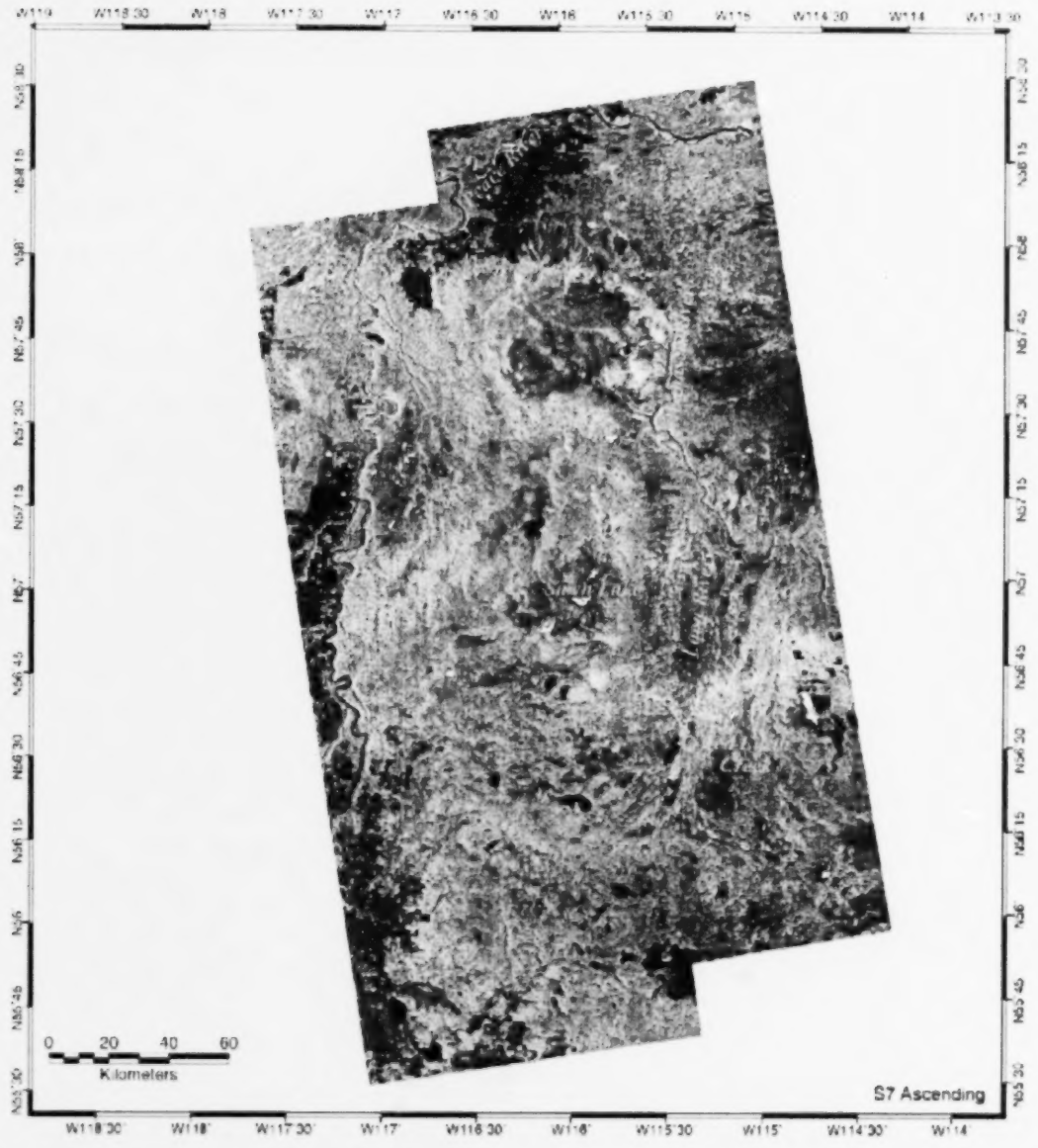

Figure 10. Mosaic of six filtered RADARSAT-1 S7 Ascending scenes.

Figure 11. Mosaic of six filtered RADARSAT-1 S7 Descending scenes.

Statistical analysis of image components extracted from multi-band, quad-polarimetric radar acquired during the SIR-C/X-SAR mission has yielded useful results for lithological mapping (Price, 1999).

Table 1. RADARSAT-1 multi-band image MOSAIC_S1S7 PCA statistics

	S1Asc	S1Des	S7Asc	S7Des
Null Cells	275408272	277384560	353489424	368787152
Non-Null Cells	409037456	407061168	330956304	315658576
Area In Hectares	6391210.250	6360330.750	5171192.250	4932165.250
Area In Acres	15793025.653	15716720.741	12778295.294	12187646.670
	S1Asc	S1Des	S7Asc	S7Des
Minimum	1.000	1.000	1.000	1.000
Maximum	255.000	255.000	255.000	255.000
Mean	111.482	110.749	112.074	113.936
Median	111.000	108.000	114.000	117.000
Std. Dev.	24.124	24.069	21.842	27.543
Std. Dev. (n-1)	24.124	24.069	21.842	27.543
Corr. Eigenval.	2.131	0.807	0.715	0.346
Cov. Eigenval.	1308.964	486.950	394.261	206.810
Correlation Matrix	S1Asc	S1Des	S7Asc	S7Des
S1Asc	1.000	0.263	0.325	0.251
S1Des	0.263	1.000	0.292	0.484
S7Asc	0.325	0.292	1.000	0.596
S7Des	0.251	0.484	0.596	1.000
Corr. Eigenvectors	PC1	PC2	PC3	PC4
S1Asc	0.392	-0.902	-0.105	-0.148
S1Des	0.476	0.243	-0.777	0.334
S7Asc	0.538	0.068	0.603	0.585
S7Des	0.574	0.351	0.150	-0.724
Covariance Matrix	S1Asc	S1Des	S7Asc	S7Des
S1Asc	581.965	152.451	171.491	166.489
S1Des	152.451	579.335	153.546	320.887
S7Asc	171.491	153.546	477.055	358.801
S7Des	166.489	320.887	358.801	758.631
Cov. Eigenvectors	PC1	PC2	PC3	PC4
S1Asc	0.358	-0.914	-0.010	0.191
S1Des	0.465	0.116	0.833	-0.276
S7Asc	0.450	0.027	-0.500	-0.739
S7Des	0.673	0.388	-0.236	0.584

Based on the same multi-band processing approach, PCA was applied to the RADARSAT-1 S1A, S1D, S7A and S7D mosaic images combined into a single multi-band image. Grunsky (2002) applied principal components analysis to two sets of incidence angles (ascending/descending) as a method to distinguish features whose responses were sensitive to differences in incidence angles.

2.1 RADARSAT-1 Statistical Processing

As a first step in the analysis, a multi-band image (MOSAIC_S1-S7) was created using the mosaic images MOSAIC_S1A, MOSAIC_S1D, MOSAIC_S7A and MOSAIC_S7D, respectively assigned to bands 1, 2, 3 and 4. The computed statistics for each band of the MOSAIC_S1-S7 image are given in Table 1. The backscatter correlation of the different bands due to different incidence angles and viewing geometries is shown in Figure 12. It can be observed from Table 1 that the strongest correlation among the mosaic bands is for bands S7A and S7D (r=0.596), which implies a high degree of data redundancy between the two images. This effect could be attributed to the shallow incidence angle characterizing the S7 Mode, which results in a reduced contrast in the image backscatter response and reduced perception of the topography. The positive correlation observed for bands 1 and 3 (r=0.325) and bands 2 and 4 (r=0.484) is clearly displayed in the scatter plots in Figure 12, and it outlines the data redundancy between bands/images acquired with the same orbit configuration. It is worth noting that the difference in incidence angles shows some degree of correlation.

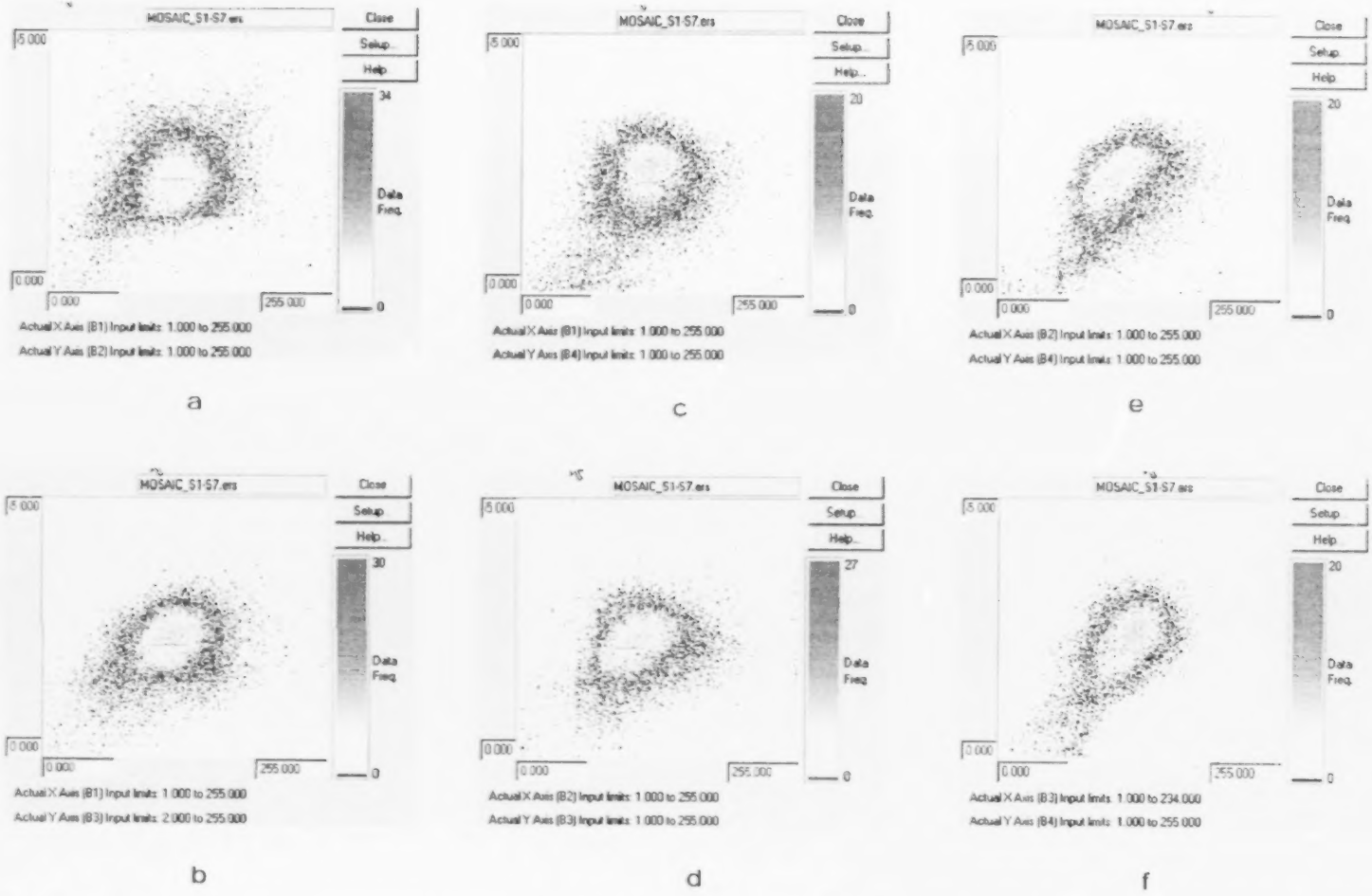
MOSAIC_S1-S7.ers
Close
Setup...
Help
Data Freq.
Actual X Axis (B1) Input limits: 1.000 to 255.000
Actual Y Axis (B2) Input limits: 1.000 to 255.000
a
Actual X Axis (B1) Input limits: 1.000 to 255.000
Actual Y Axis (B4) Input limits: 1.000 to 255.000
c
Actual X Axis (B2) Input limits: 1.000 to 255.000
Actual Y Axis (B4) Input limits: 1.000 to 255.000
e
Actual X Axis (B1) Input limits: 1.000 to 255.000
Actual Y Axis (B3) Input limits: 2.000 to 255.000
b
Actual X Axis (B2) Input limits: 1.000 to 255.000
Actual Y Axis (B3) Input limits: 1.000 to 255.000
d
Actual X Axis (B3) Input limits: 1.000 to 234.000
Actual Y Axis (B4) Input limits: 1.000 to 255.000
f

Figure 12. Scattergrams of multi-beam RADARSAT-1 S1/S7 Ascending/Descending imagery. a) S1A vs. S1D, b) S1A vs. S7A, c) S1A vs. S7D, d) S1D vs. S7A, e) S1D vs. S7D, f) S7A vs. S7D.

2.2 RADARSAT-1 Principal Component Imagery

The result of the PCA applied to the MOSAIC_S1-S7 multi-band image defines an intersection area that corresponds to the common spatial coverage of the input bands 1, 2, 3 and 4, as shown in Figure 13. This intersection area has defined the extent of the Buffalo Head Hills study area.

The application of the PCA defines four new image bands/components, which are identified as PC1, PC2, PC3 and PC4 in Table 1. The four image components are identified as linear combination of component loadings deriving from the input data distribution. The examination of the covariance eigenvectors of the PC transformation in Table 1 indicates the relative contribution of the input bands to each RADARSAT-1 PC's band/image. Positive values indicate positive association and reflect the magnitude of the input band data information within each component. Negative values indicate an inverse relationship between the input band data distribution and the component.

The first principal component, RADARSAT-1 PC1 (Figure 14), contains all positive and generally high weights from all the input bands. The higher weights are given by band 2 (S1D) (0.465) and band 4 (S7D) (0.673). The latter represents the higher weight in the image and is probably responsible for the subdued topographic perception and smoothed aspect of the image. The high contribution of band 2 seems to induce good brightness contrast and texture variability in the image along the Buffalo Head Hills edges. Intermediate weights are given by band 3 (S7A) (r= 0.450), inducing tone variation, and band 1 (S1A) (r= 0.358), probably contributing to impart texture input to the image. Overall, the image is characterized by good tone variation and textural information is preserved, but smoother than the input images.

The second principal component, RADARSAT-1 PC2 (Figure 15), contains a highly negative weight from band 1 (-0.914), which represents an inverse contribution to the image in terms of tone variability. Highest weights are derived from contribution of band 4 (0.388) and band 2 (0.116). This results in an optimal combination in the image, which emphasizes topographic perception, contrast and textural variability. The contribution of band 3 (0.027) is minimal and possibly imparts tone variation. The image is overall characterized by good topographic perception, texture and tone variability. The third principal component, RADARSAT-1 PC3 (Figure 16), contains one positive high weight due to the contribution of band 2 (0.833), whereas the other weights are all negative: band1 (-0.010), band 3 (-0.500) and band 4 (-0.236). In this image the topographic perception is very well emphasized due to the contribution of band 2. However, the inverse contribution from bands 1, 2 and 3 seem to determine a reduced "brightness" in the overall image, which results in a darker image tone. The image shows low tone variation, but extremely well defined drainage patterns due to the high contrast along the drainage and the rich texture in the overall image.

The fourth principal component, RADARSAT-1 PC4 (Figure 17), contains two positive contributions from band 1 (0.191) and band 4 (0.584) and two negative contributions from band 2 (-0.276) and band 3 (-0.739). The image is likely represented by a high level of noise; however, the main drainage is still recognized, and although diffuse, tone variation and texture information are observed in the eastern part of the image, in the Peerless Uplands region, and in the northern part of the area. Abrupt tone variations can be observed across the image, which in some cases can be related with possible structural features, but as well represent induced artefacts from the processing.

2.3 Statistics of RADARSAT-1 PC Imagery

A multi-band image, PC-MOSAIC_S1-S7, has been created using the single principal components

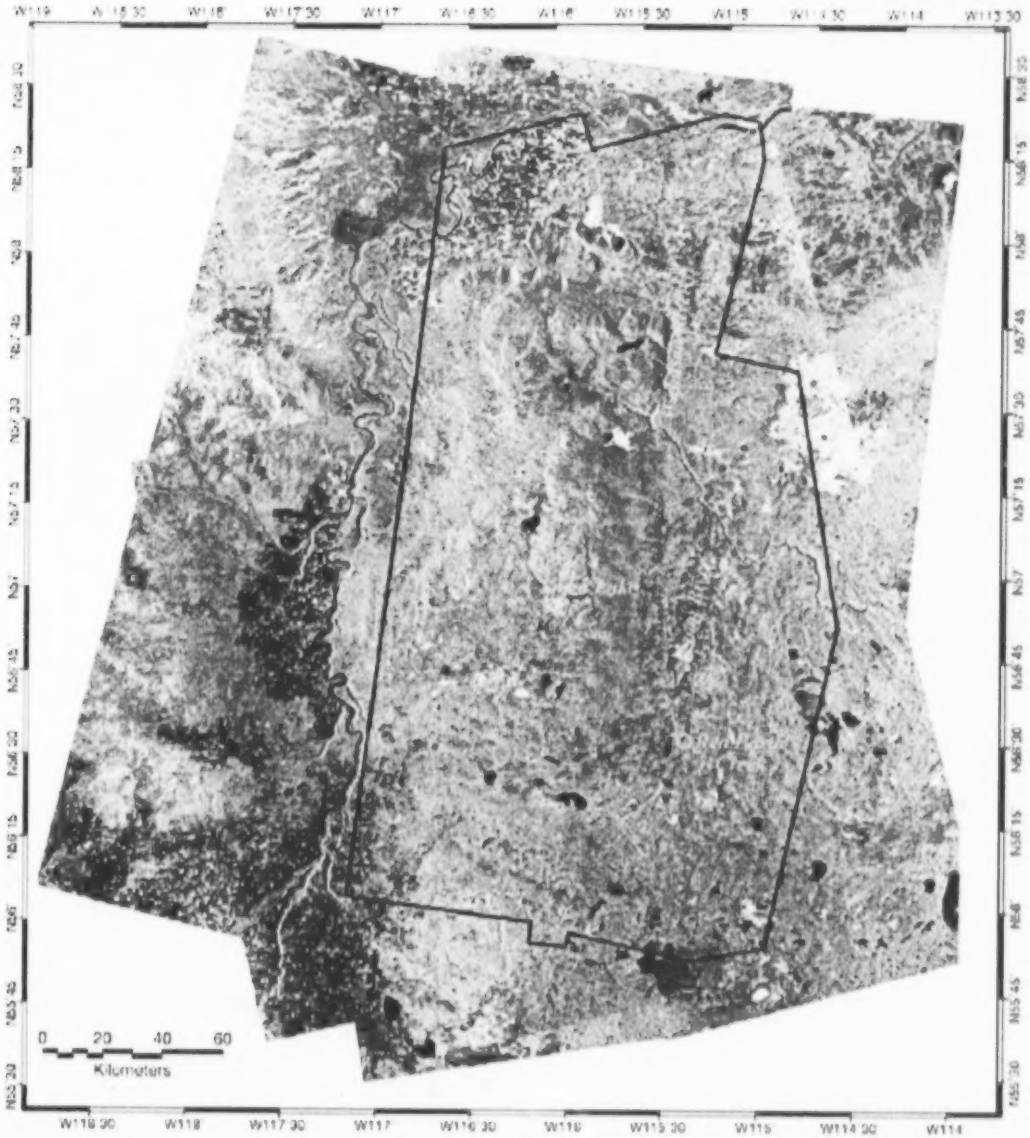

Figure 13. Mosaic coverage and intersection of S1-S7 ascending and descending RADARSAT-1 imagery.

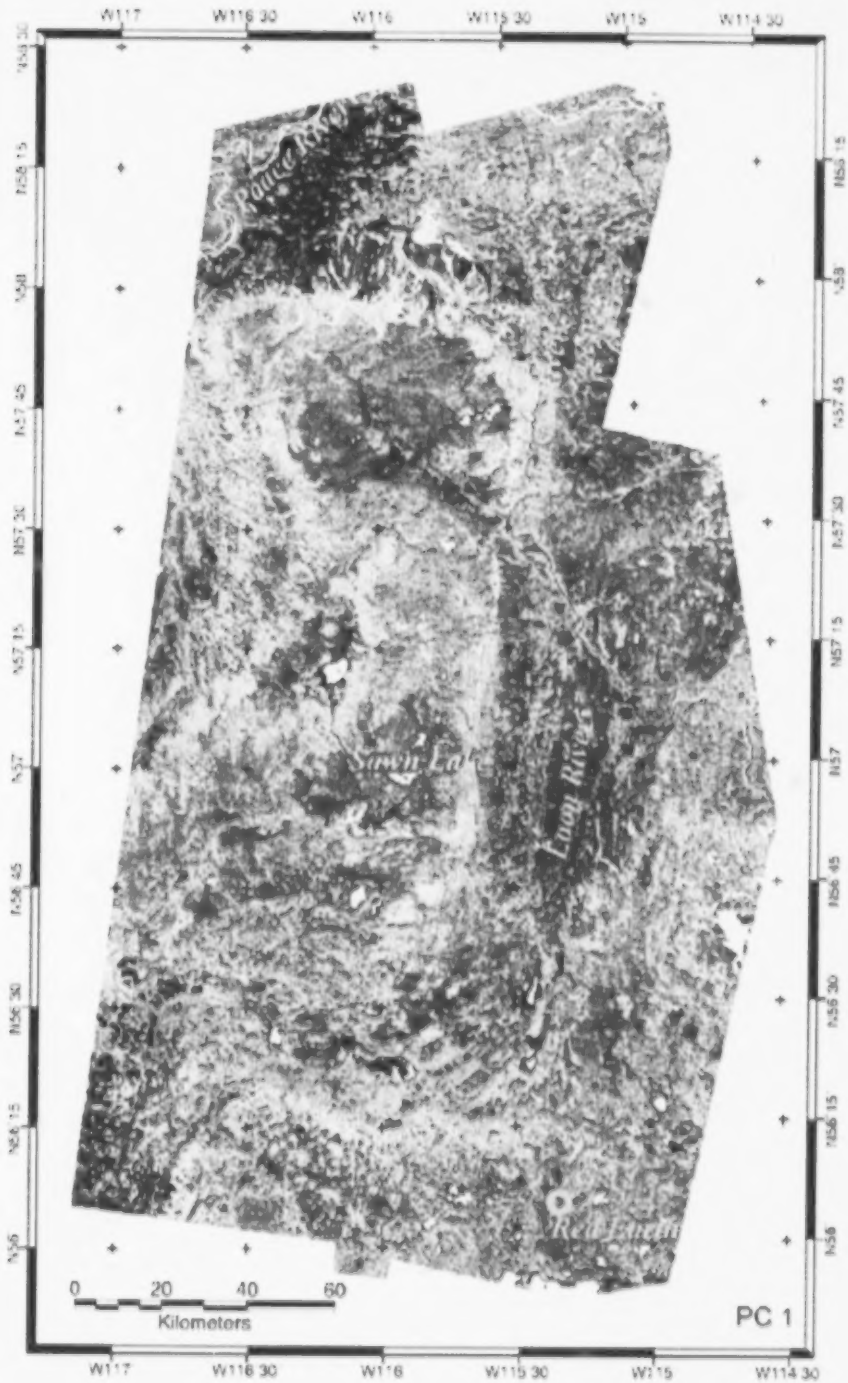

Figure 14. First Principal Component (PC1) from multi-beam RADARSAT-1 imagery.

Figure 15. Second Principal Component (PC2) from multi-beam RADARSAT-1 imagery.

Figure 16. Third Principal Component (PC3) from multi-beam RADARSAT-1 imagery.

Figure 17. Fourth Principal Component (PC4) from multi-beam RADARSAT-1 imagery.

RADARSAT-1 PC1, RADARSAT-1 PC2, RADARSAT-1 PC3 and RADARSAT-1 PC4. The computed statistics of the PC-MOSAIC_S1-S7 image for each band are given in Table 2, and a visual impression of the correlation of the RADARSAT-1 PC imagery is provided Figure 18. As expected, the principal component scatter plots show zero to very little correlation among the different RADARSAT-1 PC bands, which confirms the unique characteristics of each image, and therefore, the potentiality to emphasize independent characteristic features from the source data.

Table 2. RADARSAT-1 PC multi-band image PC_MOSAIC_S1-S7 statistics

REGION: RADARSAT-1 Pcmask

	S1Asc	S1Des	S7Asc	S7Des
Null Cells	3881936	3882160	3881904	3900816
Non-Null Cells	220006624	220006400	220006656	219987744
Area In Hectares	3437603.500	3437600.000	3437604.000	3437308.500
Area In Acres	8494503.879	8494495.230	8494505.115	8493774.918

Covariance Matrix	S1Asc	S1Des	S7Asc	S7Des
Minimum	1.000	1.000	24.000	1.000
Maximum	254.000	255.000	255.000	187.000
Mean	111.135	153.725	150.565	68.078
Median	113.000	155.000	149.000	68.000
Std. Dev.	18.666	19.866	15.870	11.644
Std. Dev. (n-1)	18.666	19.866	15.870	11.644
Corr. Eigenval.	1.011	1.003	1.000	0.986
Cov. Eigenval.	394.730	348.440	251.764	135.579

Correlation Matrix	S1Asc	S1Des	S7Asc	S7Des
S1Asc	1.000	0.001	0.003	0.000
S1Des	0.001	1.000	-0.011	-0.004
S7Asc	0.003	-0.011	1.000	-0.004
S7Des	0.000	-0.004	-0.004	1.000

Corr. Eigenvectors	PC1	PC2	PC3	PC4
S1Asc	0.124	-0.210	-0.956	0.164
S1Des	-0.695	-0.308	-0.132	-0.637
S7Asc	0.709	-0.280	0.042	-0.646
S7Des	0.012	0.885	-0.259	-0.387

Covariance Matrix	S1Asc	S1Des	S7Asc	S7Des
S1Asc	348.435	0.247	0.756	0.092
S1Des	0.247	394.645	-3.392	-0.959
S7Asc	0.756	-3.392	251.846	-0.732
S7Des	0.092	-0.959	-0.732	135.587

Cov. Eigenvectors	PC1	PC2	PC3	PC4
S1Asc	-0.005	-1.000	0.008	-0.000
S1Des	-1.000	0.005	-0.024	0.004
S7Asc	0.024	-0.008	-1.000	0.006
S7Des	0.004	-0.000	0.006	1.000

3 Structural Interpretation of RADARSAT-1 Principal Component Images

The method applied in the interpretation of the RADARSAT-1 PC's imagery consists of visual pattern recognition using tone, contrast and textural variations. These image characteristics are determined by the surface roughness, soil dielectric properties, slope attitude and vegetation coverage (Evans et al., 1986; Price, 1999) affecting the radar backscatter. At the C-band radar wavelength and the Horizontal-Horizontal (HH) polarization used by RADARSAT-1, most of the light interaction occurs within the top of the relatively uniform forest canopy, which directly reflects either changes of erosional escarpment due to variation of resistant and recessive lithological units (Brown et al. 1996; Paganelli and Rivard, 2001), or structural escarpments. Image tone, contrast and texture variation are emphasized by the appropriate look direction and incidence angle inherent in the RADARSAT-1 image acquisition.

In each of the RADARSAT-1 PC images, linear features are readily identified, some of which could be interpreted as structurally controlled fault or lineament patterns. They include structures outlined as a

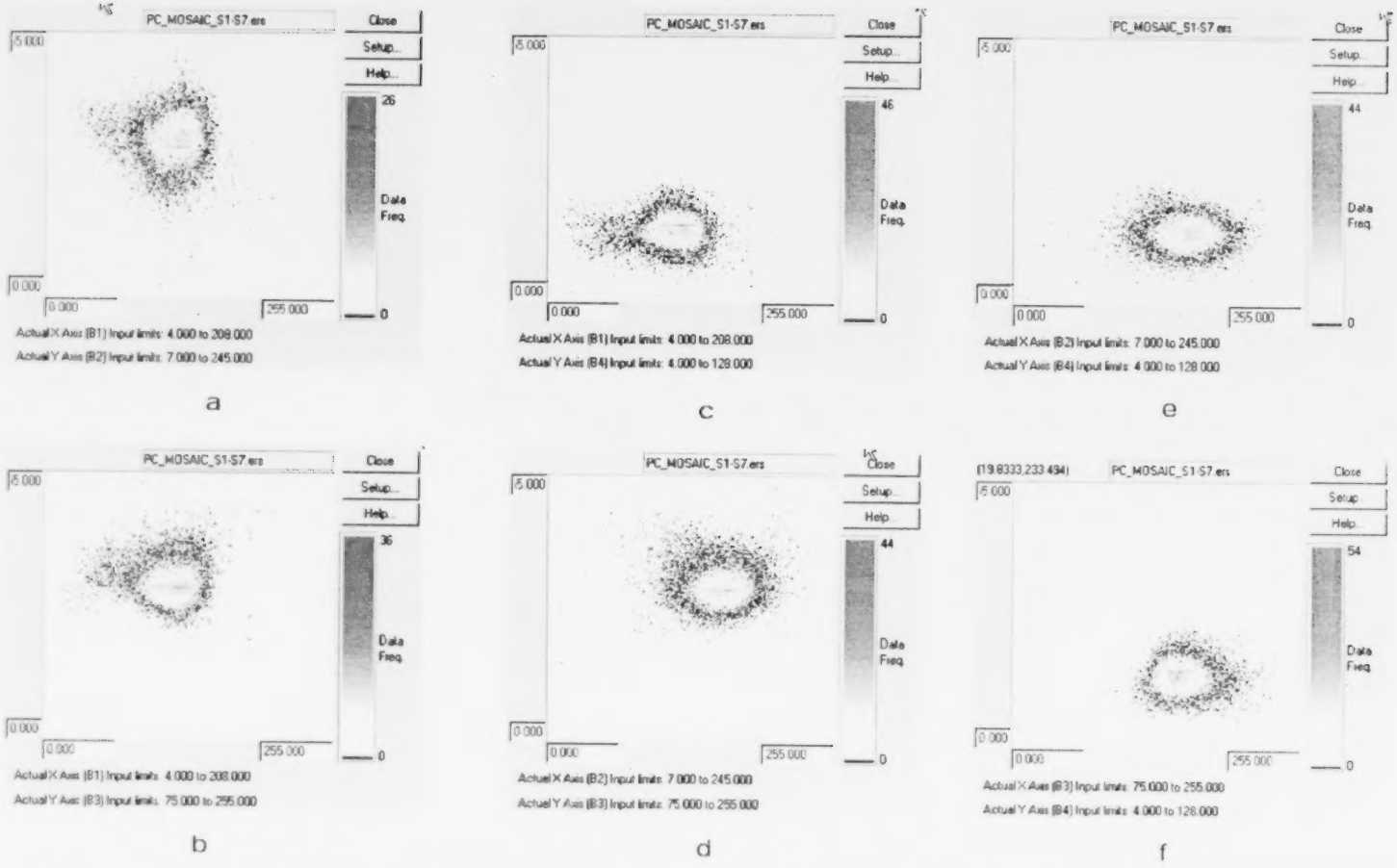
PC_MOSAIC_S1-S7.ers
Close
Setup...
Help...
Data Freq.
Actual X Axis (B1) Input limits: 4.000 to 208.000
Actual Y Axis (B2) Input limits: 7.000 to 245.000
a
Actual X Axis (B1) Input limits: 4.000 to 208.000
Actual Y Axis (B4) Input limits: 4.000 to 128.000
c
Actual X Axis (B2) Input limits: 7.000 to 245.000
Actual Y Axis (B4) Input limits: 4.000 to 128.000
e
Actual X Axis (B1) Input limits: 4.000 to 208.000
Actual Y Axis (B3) Input limits: 75.000 to 255.000
b
Actual X Axis (B2) Input limits: 7.000 to 245.000
Actual Y Axis (B3) Input limits: 75.000 to 255.000
d
Actual X Axis (B3) Input limits: 75.000 to 255.000
Actual Y Axis (B4) Input limits: 4.000 to 128.000
f

Figure 18. Scattergrams of principal components derived from multi-beam RADARSAT-1 S1/S7 Ascending/Descending imagery. a) PC1 vs. PC2, b) PC1 vs. PC3, c) PC1 vs. PC4, d) PC2 vs. PC3, e) PC2 vs. PC4, f) PC3 vs. PC4.

result of contrast and shadowing effects induced by topographic variation and/or drainage patterns and textural variations induced by dielectric properties of surface materials related to lithological and/or vegetation canopy variations. The latter are, in turn, related to soil conditions and bedrock characteristics.

3.1 RADARSAT-1 PC Structural Interpretation

To evaluate the validity of RADARSAT-1 PC structural interpretation, each image was interpreted separately. This approach allows independent identification of structural features that may have variable degrees of accuracy or certainty in each image. At this time, the interpretations have been conducted visually without using automated methods of feature extraction. The application of computer-based lineament extraction techniques may be tested in the future.

Four main lineament trends have been recognized in each of the RADARSAT-1 PC images: north-northeast, northwest, northeast and east-northeast. They are described below based on recognition characteristics and spatial distribution. Intersections and offset relationships between the various lineament groups define their temporal relationships: the north-northeast lineaments are recognized as the oldest features, followed by the northwest and northeast lineaments (which possibly define a conjugate set), and finally the east-northeast lineaments. In Figure 19, the geology and drainage has been draped on the RADARSAT-1 PC2 image to aid interpretation of the data in terms of bedrock lithology and physiographic features. The locations of the known kimberlites are also displayed on the structural interpretation maps (Figures 20 to 23). Possible spatial relationships between the traced structures are discussed below.

A tentative tectonic evolution of the outlined features is provided, based on review of published literature, and previous work conducted in the Peerless Lake area by Eccles et al. (2000), which included the southeast corner of the Buffalo Head Hills. The relationship between the identified structural trends in the Buffalo Head Hills area and the development of the Peace River Arch is also discussed below.

A compilation of the outlined structural trends is shown in Figures 24 through 27 to evaluate the variability of the depicted features, and it suggests avenues for further work relating to the statistical analysis of structural orientations within the area.

The RADARSAT-1 PC structural interpretation maps of Figures 24 to 27 are also provided at 1:500 000 scale in PDF format (Maps 1 to 4).

3.2 RADARSAT-1 PC1 Structural Interpretation

The RADARSAT-1 PC1 image appears to give a good response for structural features extraction due to good contrast, tone and textural variation, but it lacks topographic contrast (Figure 20).

The north-northeast–trending lineaments are readily traced along the eastern boundary of the Buffalo Head Hills because of the contrast in brightness, texture and tone between the Buffalo Head Hills east-facing scarp and the Loon River valley; these contrasts are probably induced by topographic and surface terrain variations. The shadowing effect outlined by the drainage pattern of the Wabasca River along the northern portion of the Buffalo Head Hills eastern boundary is possibly also controlled by north-northeast–trending lineaments. Similar lineaments are observed in the western boundary of the Peerless Uplands and define drainage patterns in the northern portion of the Loon River valley, the central portion of the Buffalo Head Hills, and in the southern limit of the study area.

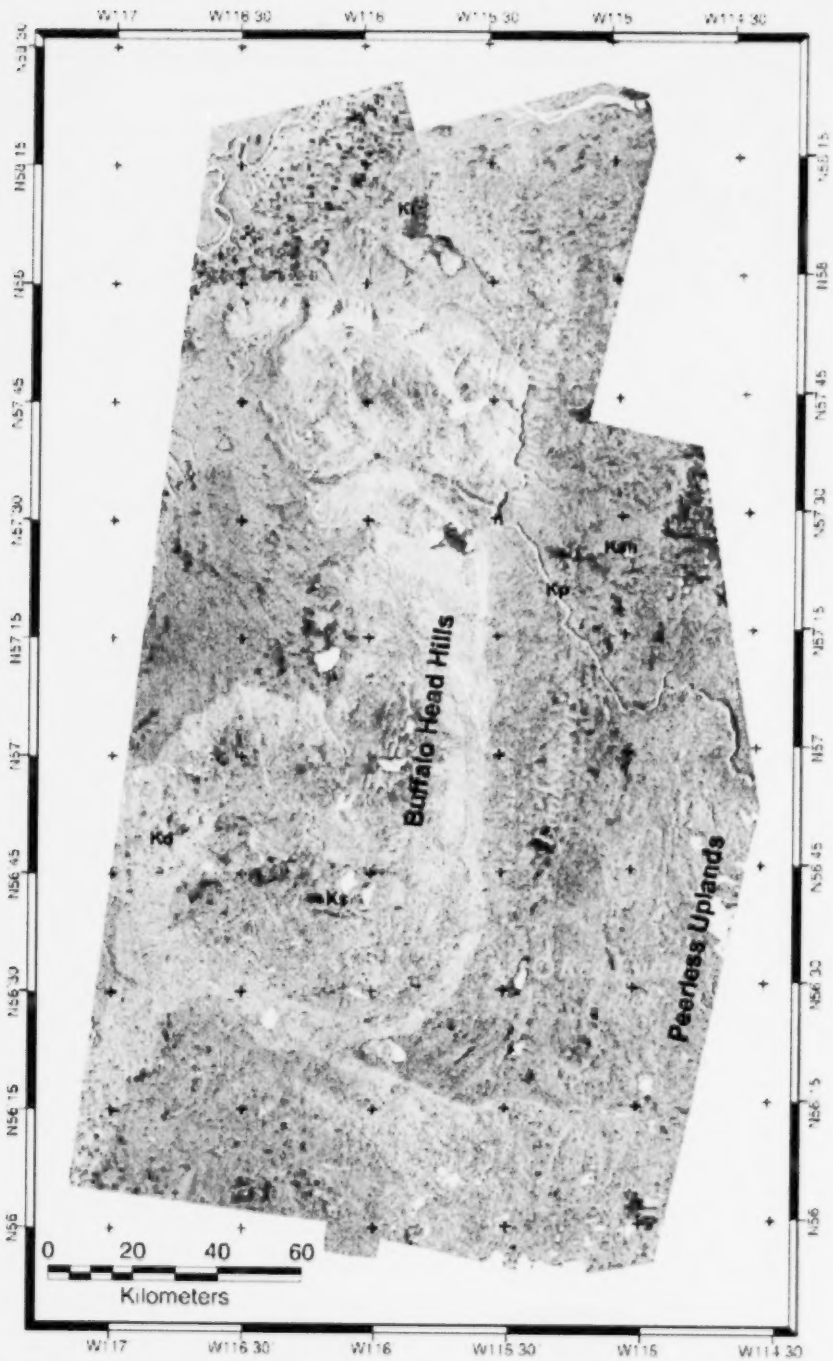

Figure 19. Geology of the Buffalo Head Hills over the second Principal Component (PC2): Kl, Loon River Formation (Lower Cretaceous); Kp, Peace River Formation (Lower Cretaceous); Ksh, Shaftesbury Formation (Lower-Upper Cretaceous); Kd, Dunvegan Formation (Upper Cretaceous); Ks, Smoky Group (Upper Cretaceous).

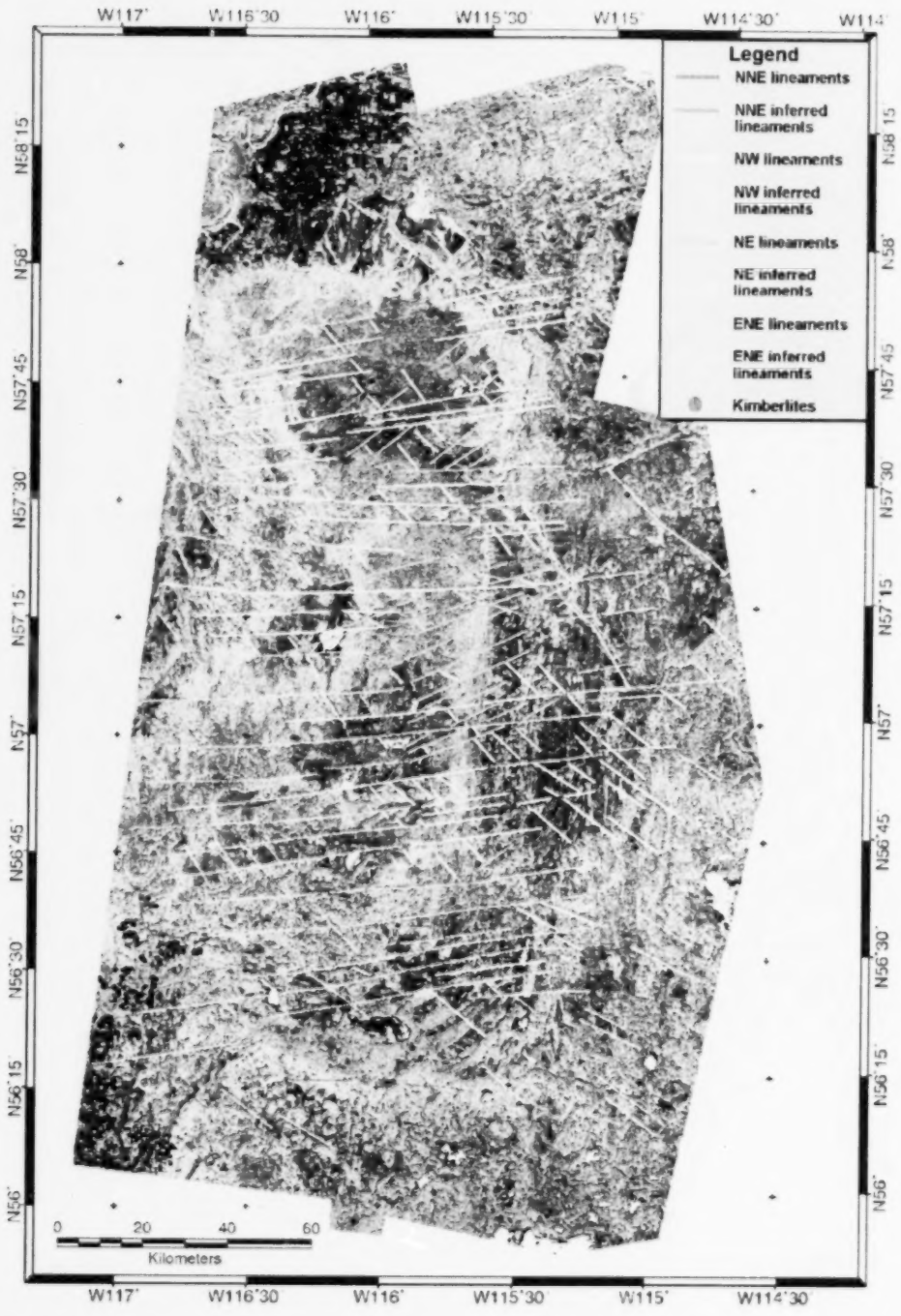

Figure 20. Principal Component 1 (PC1) with structural interpretation derived from PC1.

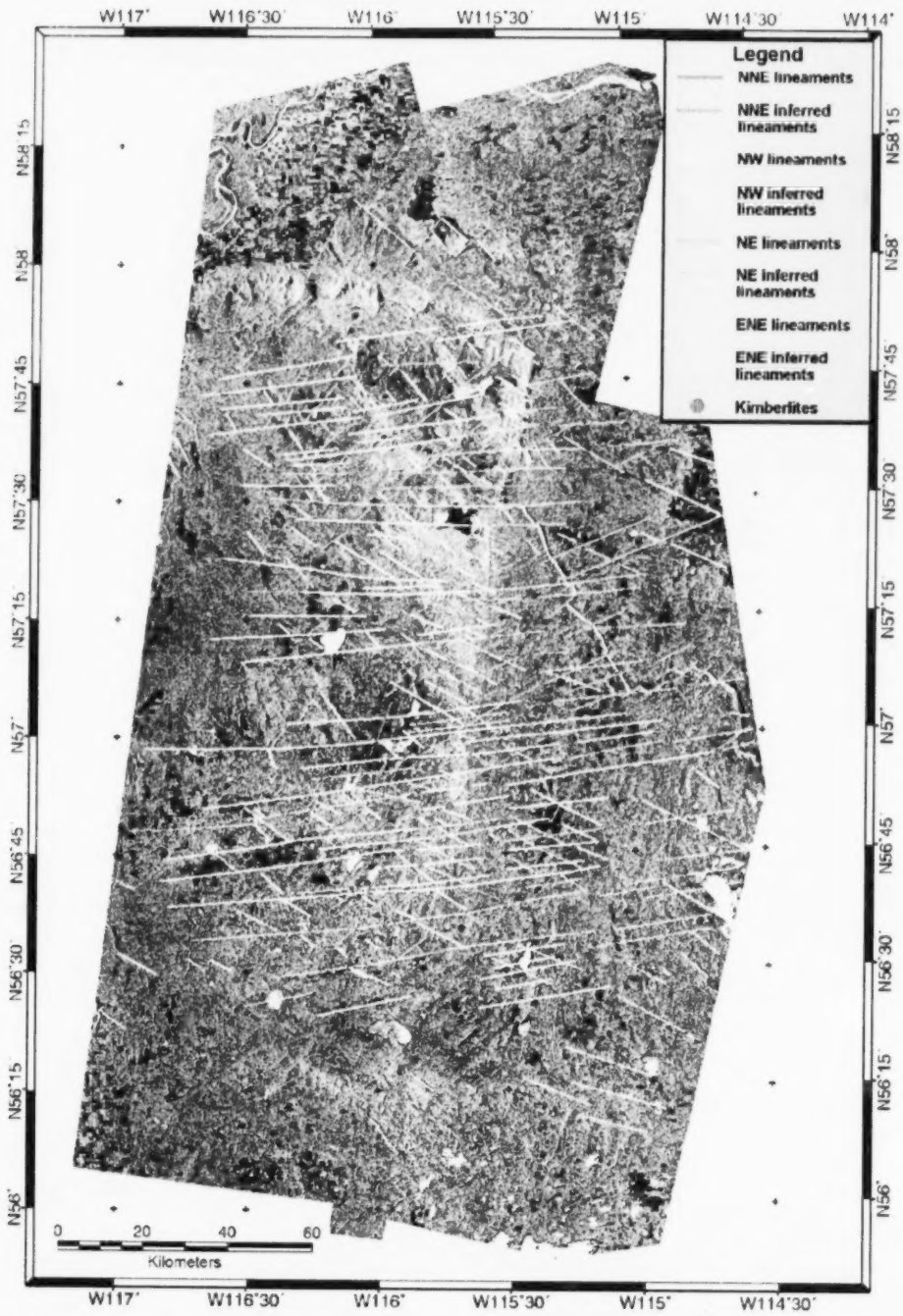

Figure 21. Principal Component 2 (PC2) with structural interpretation derived from PC2.

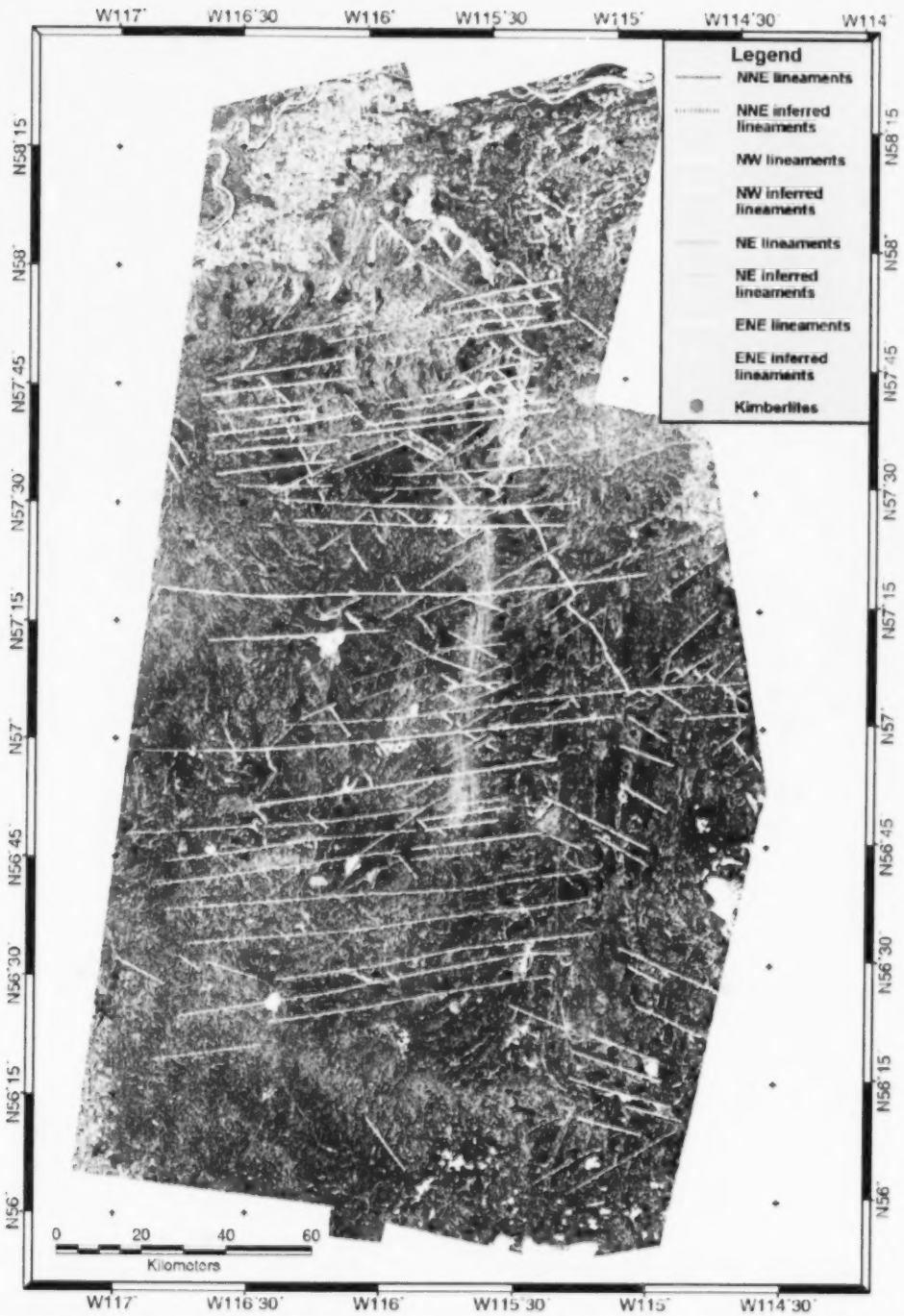

Figure 22. Principal Component 3 (PC3) with structural interpretation derived from PC3.

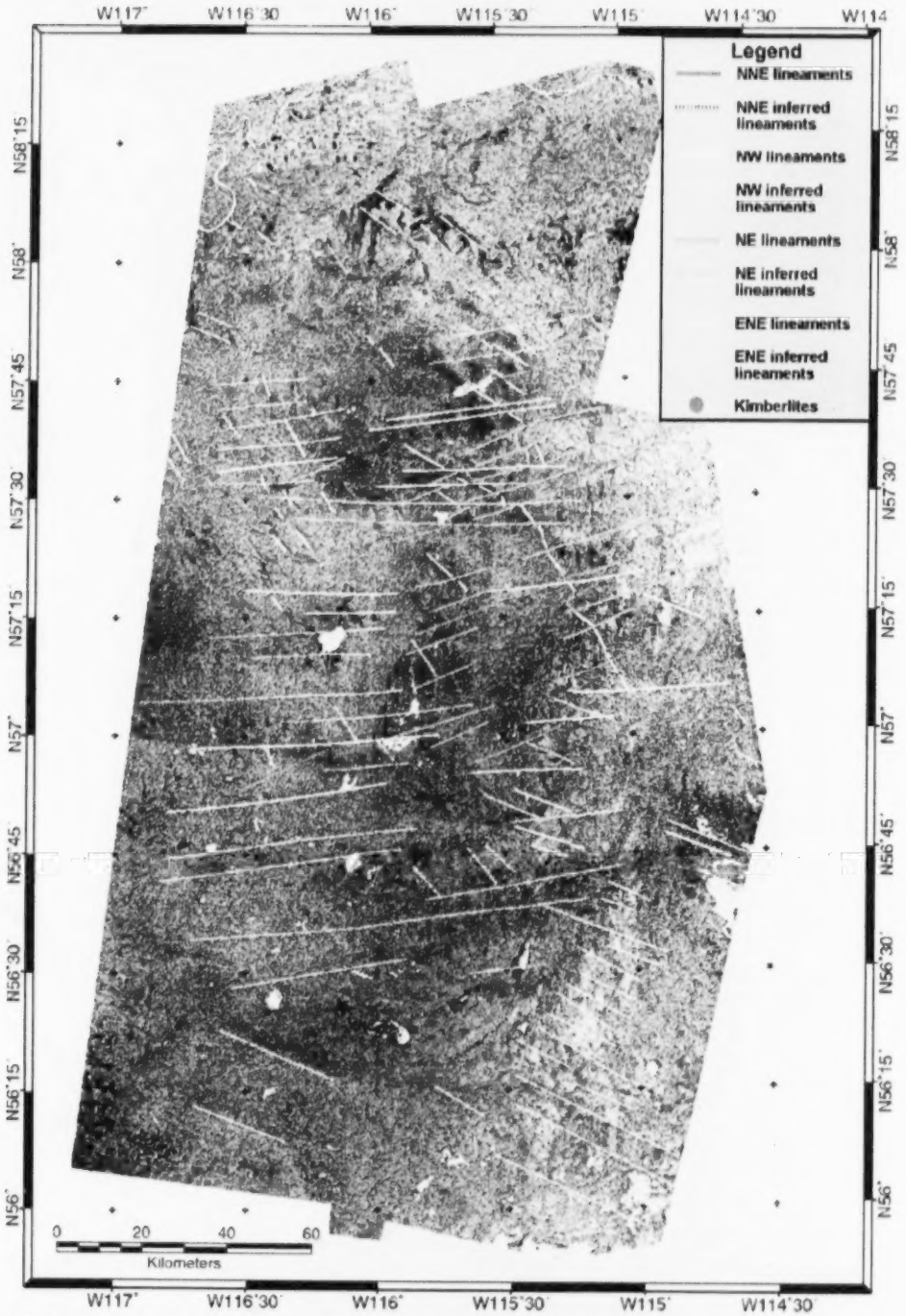

Figure 23. Pricipal Component 4 (PC4) with structural interpretation derived from PC4.

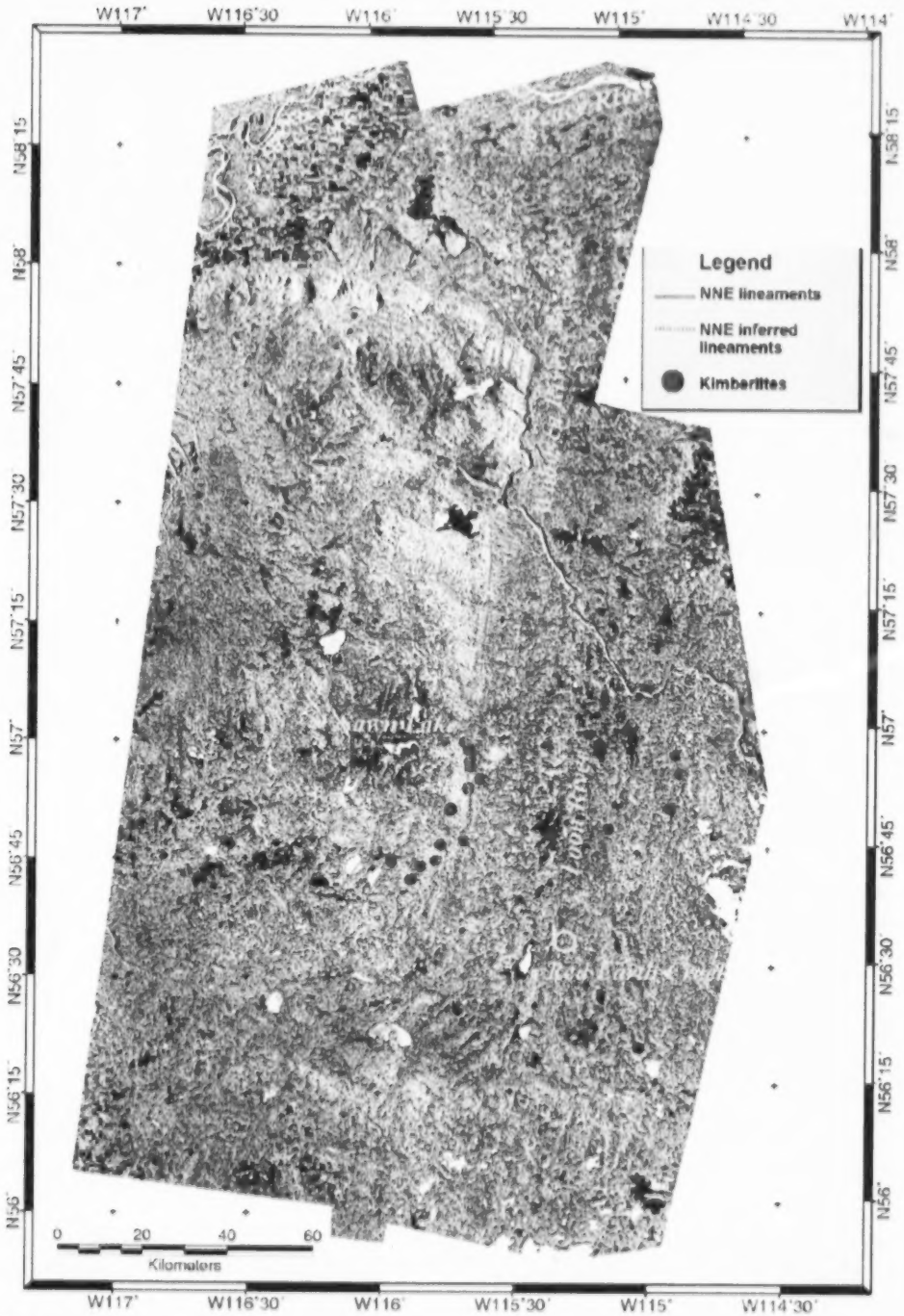

Figure 24. Principal Component 2 (PC2) with N-NE lineament compilation.

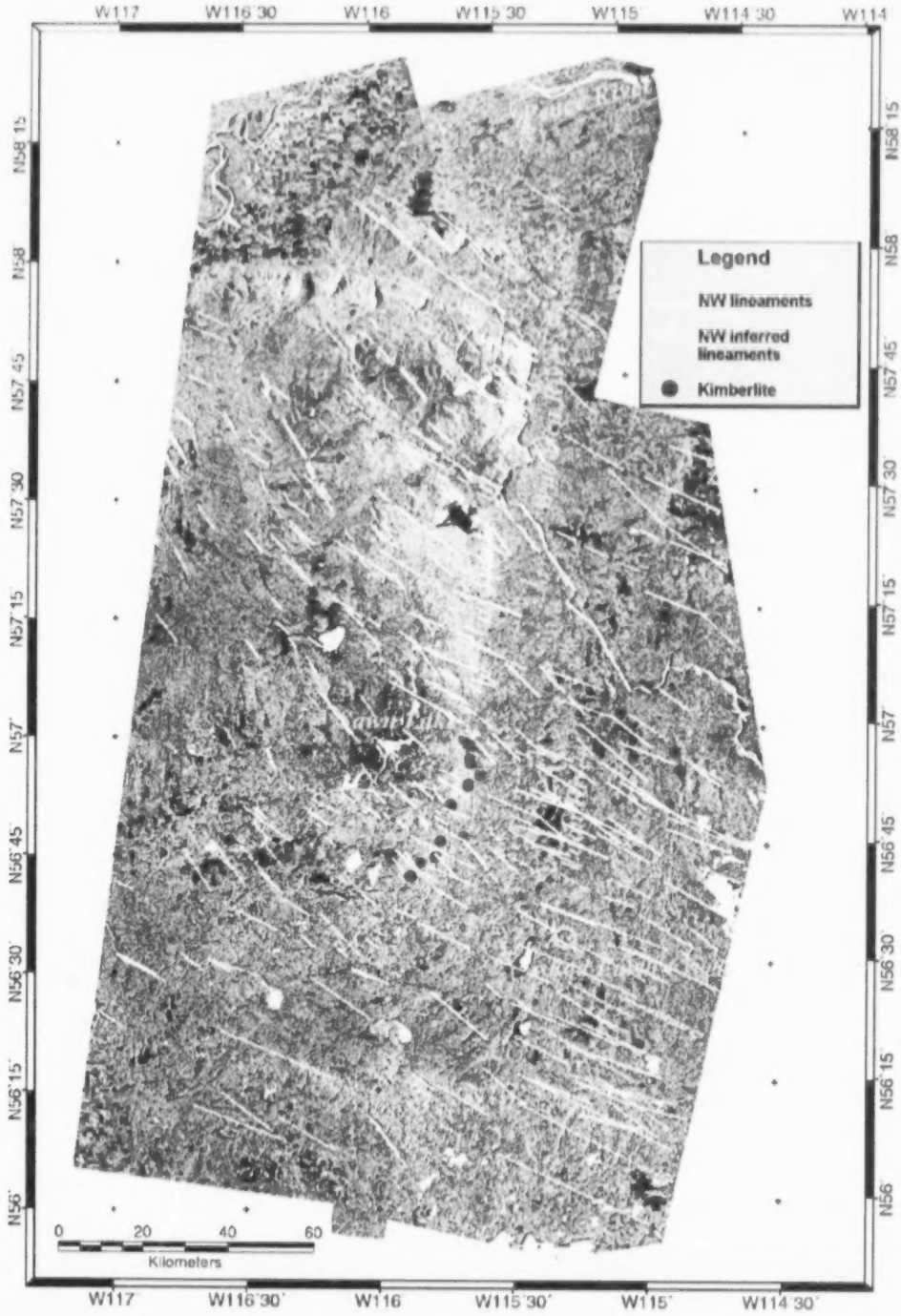

Figure 25. Principal Component 2 (PC2) with NW Lineament compilation.

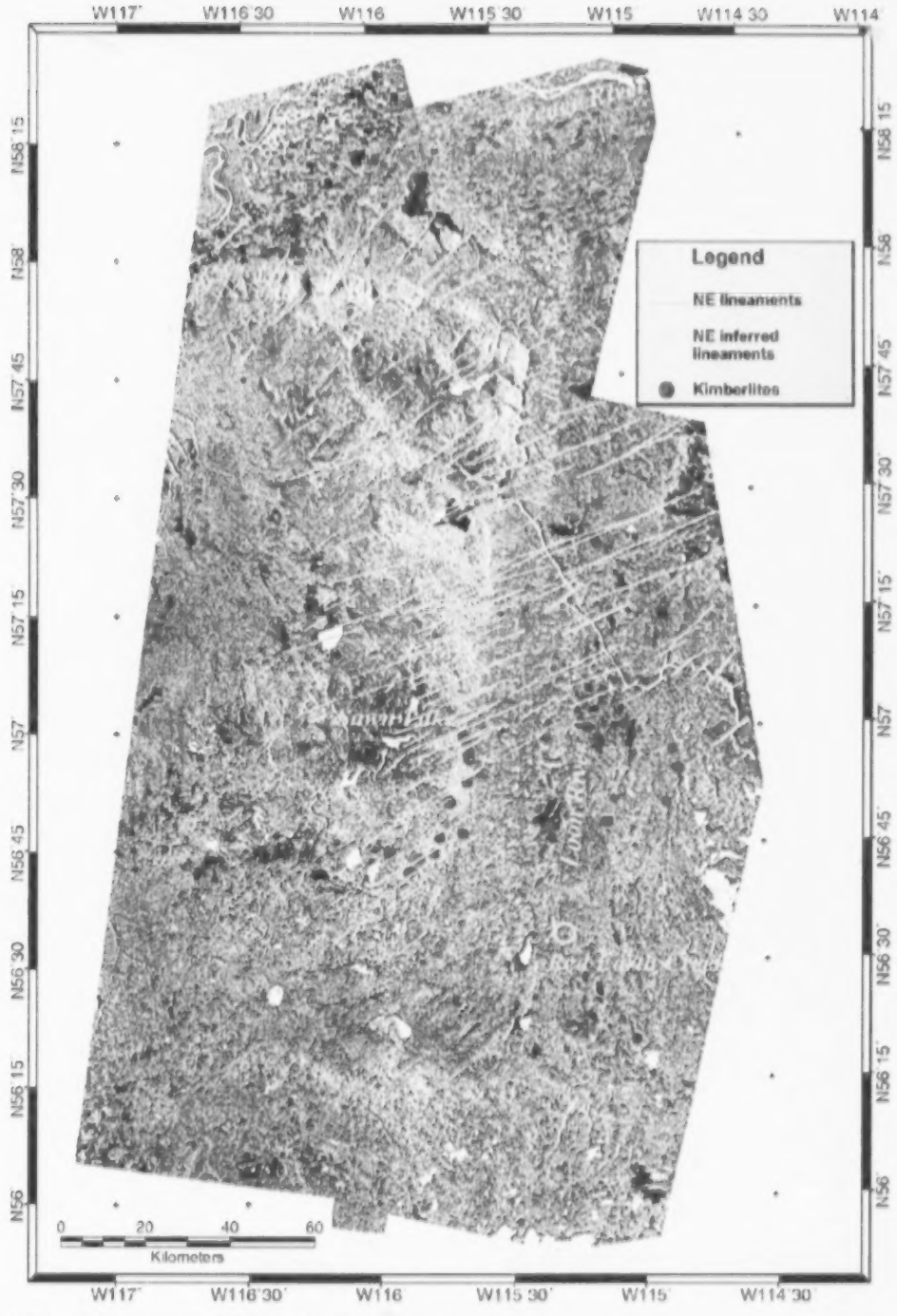

Figure 26. Principal Component 2 (PC2) with NE lineament compilation.

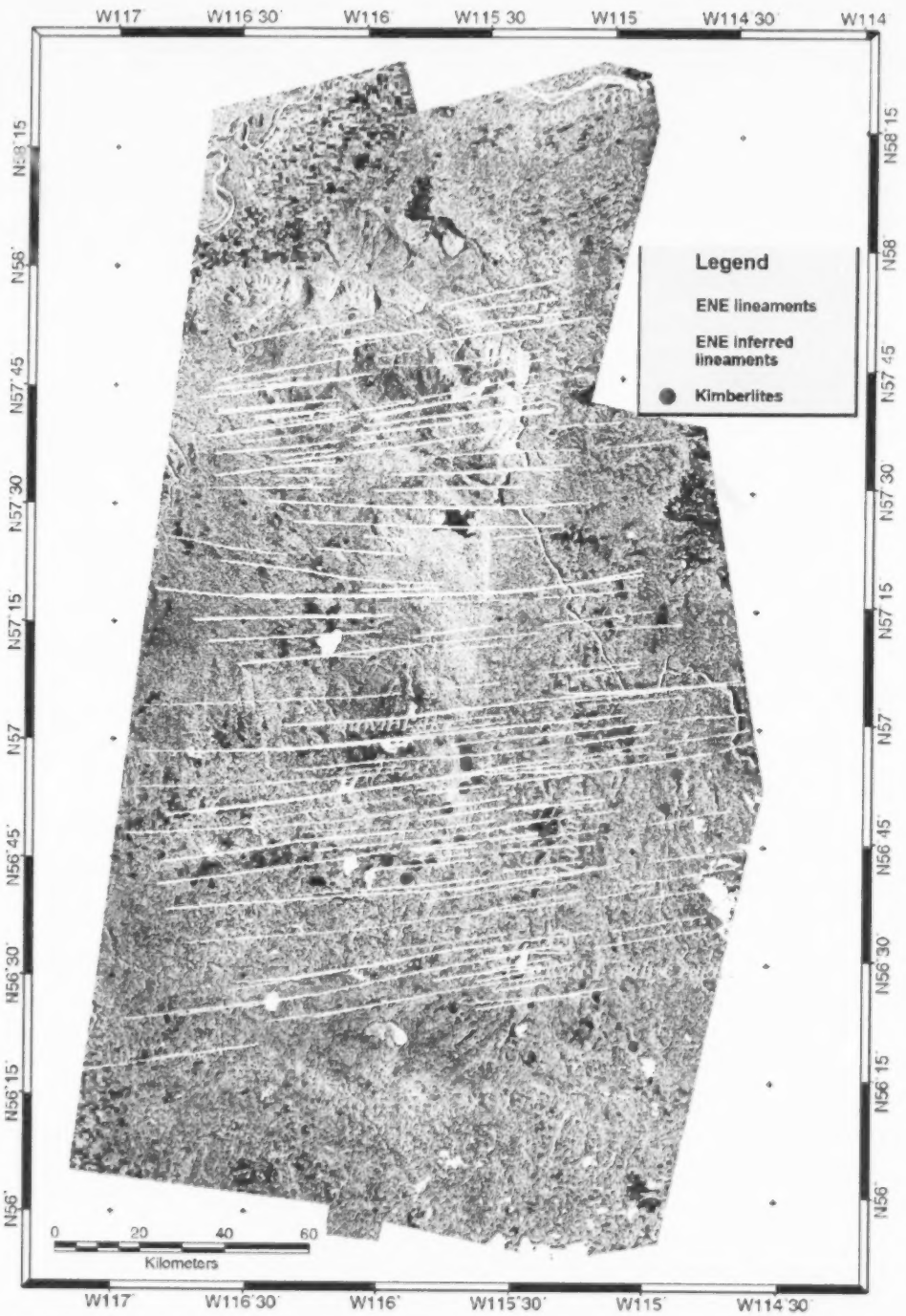

Figure 27. Principal Component 2 (PC2) with ENE lineament compilation.

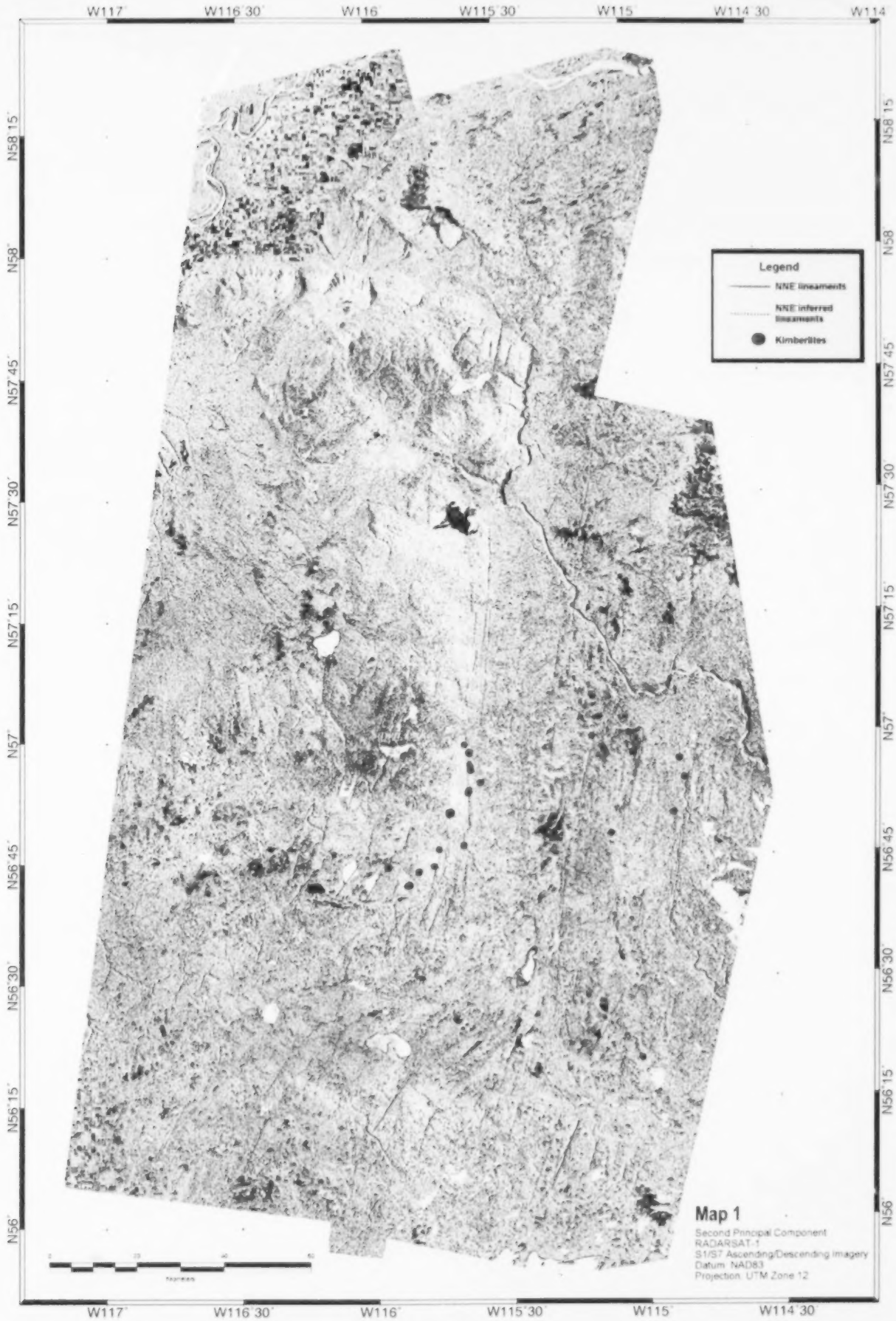
W117°
W116°30'
W116°
W115°30'
W115°
W114°30'
W114°
N58°15'
N58°
N57°45'
N57°30'
N57°15'
N57°
N56°45'
N56°30'
N56°15'
N56°
Legend
NNE lineaments
NNE inferred lineaments
Kimberlites
Map 1
Second Principal Component
RADARSAT-1
S1/S7 Ascending/Descending Imagery
Datum: NAD83
Projection: UTM Zone 12

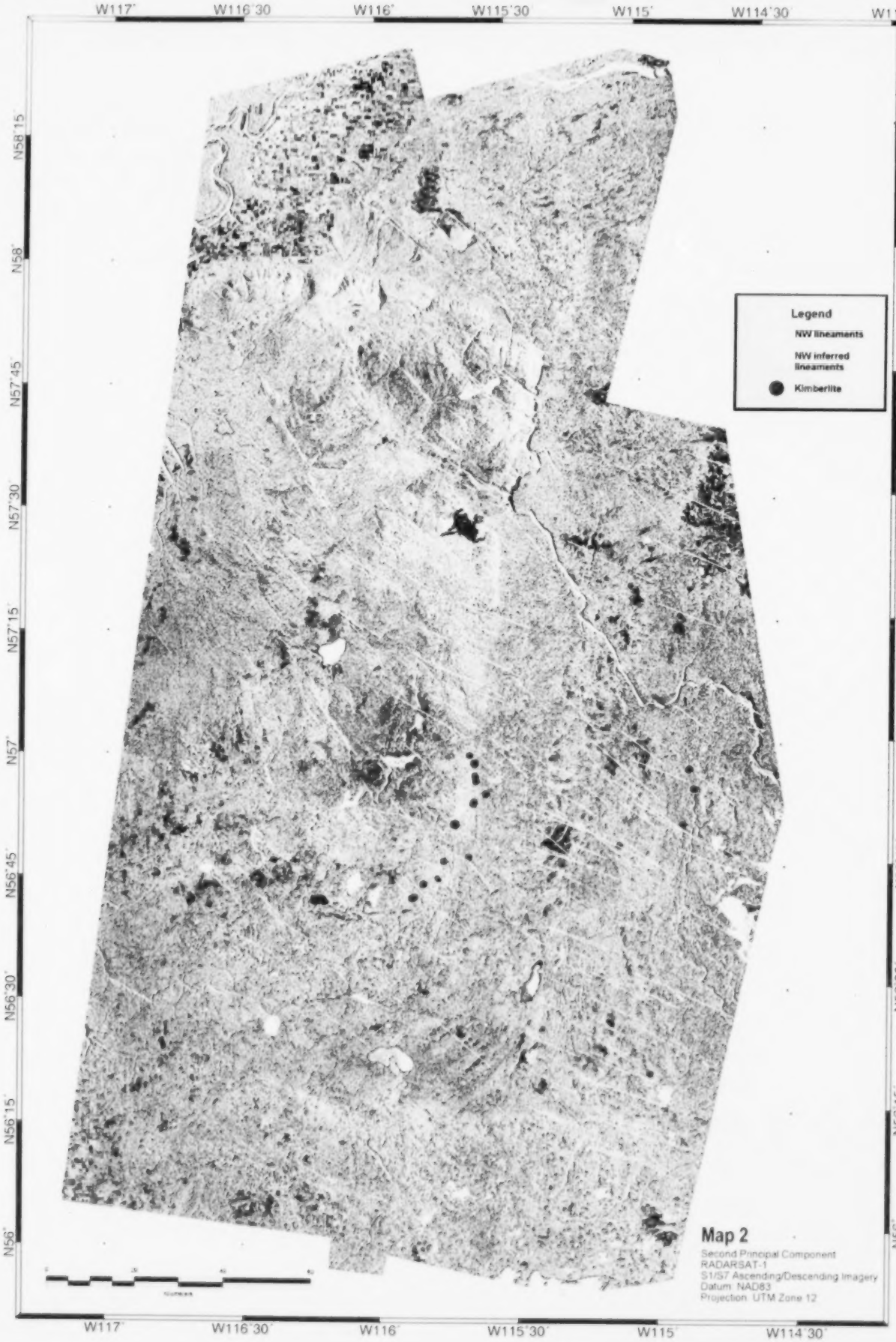
W117°
W116°30'
W116°
W115°30'
W115°
W114°30'
W114°
N58°15'
N58°
N57°45'
N57°30'
N57°15'
N57°
N56°45'
N56°30'
N56°15'
N56°
Legend
NW lineaments
NW inferred lineaments
Kimberlite
Map 2
Second Principal Component
RADARSAT-1
S1/S7 Ascending/Descending Imagery
Datum: NAD83
Projection: UTM Zone 12

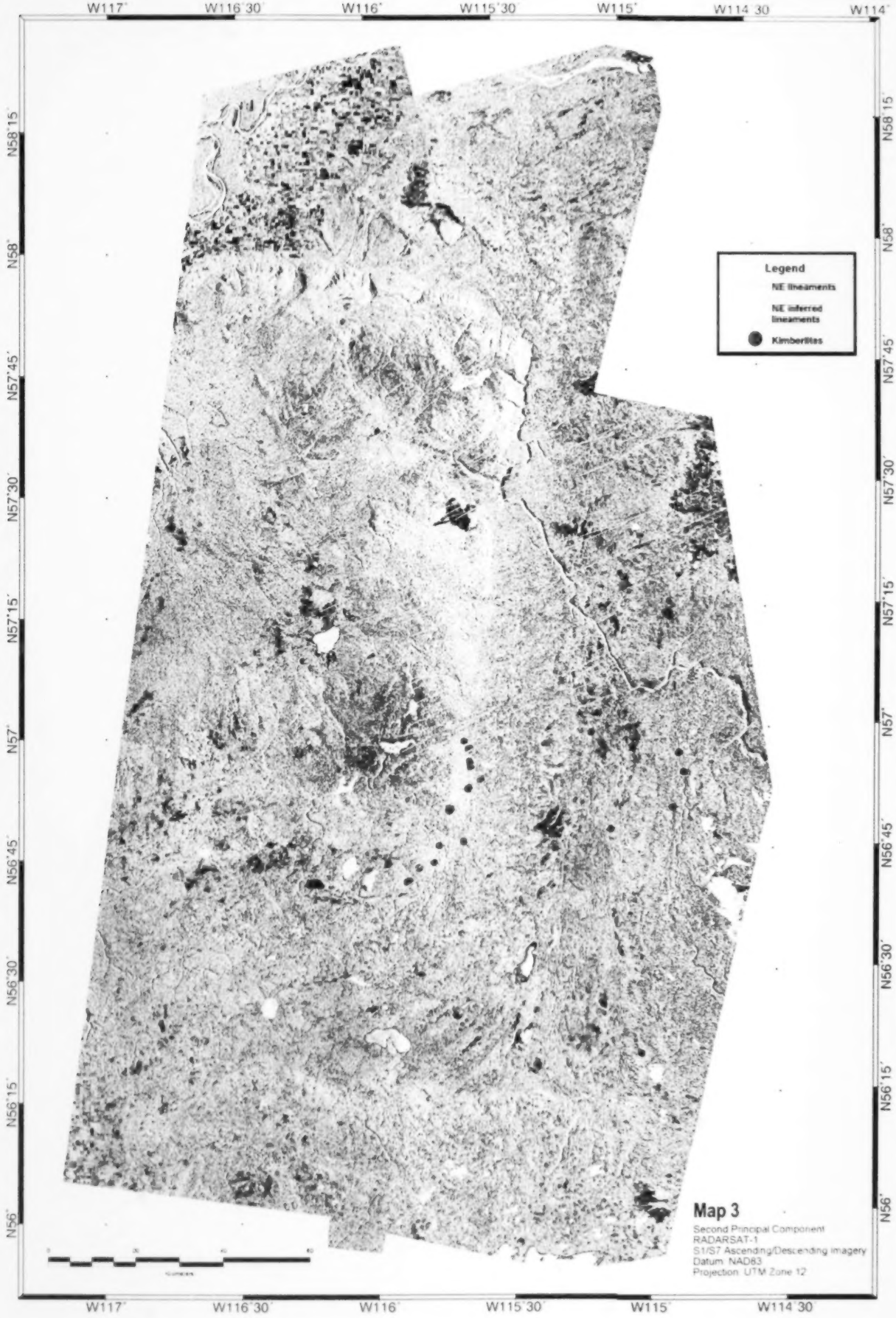
W117°
W116°30'
W116°
W115°30'
W115°
W114°30'
W114°
N58°15'
N58°
N57°45'
N57°30'
N57°15'
N57°
N56°45'
N56°30'
N56°15'
N56°
Legend
NE lineaments
NE inferred lineaments
Kimberlites
Map 3
Second Principal Component
RADARSAT-1
S1/S7 Ascending/Descending Imagery
Datum: NAD83
Projection: UTM Zone 12

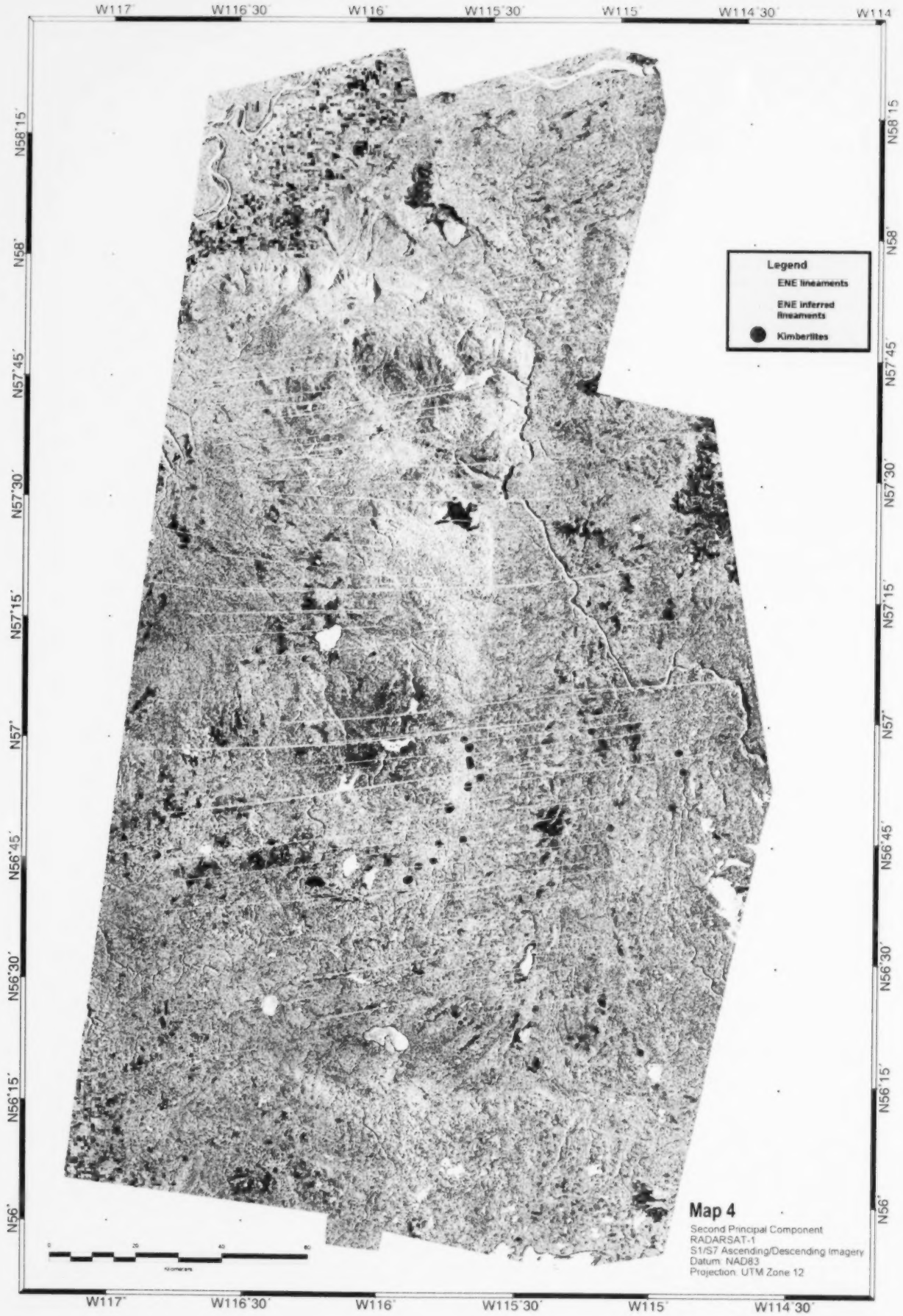
W117°
W116°30'
W116°
W115°30'
W115°
W114°30'
W114°
N58°15'
N58°
N57°45'
N57°30'
N57°15'
N57°
N56°45'
N56°30'
N56°15'
N56°
Legend
ENE lineaments
ENE inferred lineaments
Kimberlites
0
20
40
60
Kilometers
Map 4
Second Principal Component
RADARSAT-1
S1/S7 Ascending/Descending Imagery
Datum: NAD83
Projection: UTM Zone 12

The northwest-trending lineaments intersect and offset the north-northeast–trending lineaments, suggesting a relative age relationship. This lineament set can be traced throughout the study area from the southeast in the western boundary of the Peerless Uplands, through the Loon River valley, to the northwest across the Buffalo Head Hills. The offset induced by the northwest lineaments is mainly observable in the Buffalo Head Hills and Loon River valley from texture and tone variations, interpreted to be a response to lithological changes and/or structural escarpments. The highest concentrations of northwest lineaments are observed in the southeast corner of the area, the central portion of the Loon River valley, and the northern portion and western limit of the Buffalo Head Hills. The surficial drainage pattern in the western boundary of the image appears to be controlled by this linear trend. In the southeast corner of the Buffalo Head Hills, the northwest lineaments define a series of step-faults propagating toward the southwest, which can be observed due to the contrast in texture and tone variation induced by lithologic transition of the Dunvegan Formation (brighter tone) and the Smoky Group (darker tone). These features have probably determined the down-throw of the southeast corner and southern boundary of the Buffalo Head Hills to the southwest.

The northeast-trending lineaments intersect and offset the north-northeast- and northwest-trending lineaments, again indicating relative age. This lineament set can be traced mainly across the Buffalo Head Hills from the southeast corner to the northwest corner, although some lineaments extend through the Loon River Valley and a few lineaments have been traced in the Peerless Uplands. The offset induced by the northeast-trending lineaments is mainly observable along the Buffalo Head Hills eastern boundary and is visible as textural and tone variations in response to lithological changes between the Shaftesbury Formation, Dunvegan Formation and Smoky Group. The highest concentration of northeast lineaments is observed in the Buffalo Head Hills near its eastern and northern boundaries. In the northwest corner of the Buffalo Head Hills, a series of northeast lineaments are outlined by the contrast in texture and tone variation induced by the lithologic transition of the Loon River Formation (dark grey), Shaftesbury and Dunvegan formations (light grey) and the Smoky Group (medium grey). They act as step-faults propagating toward the northwest and have probably down-thrown the Buffalo Head Hills northern boundary toward the northwest. In the central portion of the Buffalo Head Hills, and along its eastern boundary, the interference between the northwest- and north-northeast–trending lineaments possibly resulted in the down-throw of the Buffalo Head Hills toward the southeast.

The east-northeast–trending lineaments intersect and offset the north-northeast-, northwest- and northeast-trending lineaments and are the youngest structural features in the area. They are regionally distributed from south to north, almost regularly spaced and can be traced throughout the Buffalo Head Hills, the Loon River valley, and part of the western limit of the Peerless Uplands. The highest concentration of east-northeast lineaments is observed in the southeast corner, southern boundary and northeast portion of the Buffalo Head Hills. The offset induced by the east-northeast–trending lineaments is mainly observable along the Buffalo Head Hills eastern boundary, again as textural and tonal variations in response to changes in soil conditions, surface roughness and forest canopy changes that may reflect lithological change between the Shaftesbury Formation, Dunvegan Formation and Smoky Group. These lineaments appear to define step-faults that down-throw the southern boundary toward the southeast and the northeast corner of the Buffalo Head Hills toward the north-northwest.

3.3 RADARSAT-1 PC2 Structural Interpretation

The RADARSAT-1 PC2 image is characterized by good topographic perception, contrast and texture variation, with moderate tone variability. Many of the same linear patterns present in the RADARSAT-1 PC1 image have been recognized, but the good topographic perception in this image facilitates the

recognition of structural features (Figure 21).

The north-northeast linear trend is well defined in this image, and additional lineaments have been traced in the Buffalo Head Hills area at its eastern edge, central part and northeast and southern corners. North-northeast–trending lineaments have also been traced in the Loon River valley where they appear to control drainage patterns in the western boundary of the Peerless Uplands and in the southern portion of the study area.

The northwest-trending lineaments can be traced throughout the study area, and new features not recognized in the RADARSAT-1 PC1 image have been traced along the eastern edge, the southeast corner, and northeastern corner of the Buffalo Head Hills. Additional features have been mapped in the western boundary of the Peerless Uplands and Loon River valley, as well as in the southwest corner of the image. In particular, northwest-trending lineaments appear to control the trend of the Wabasca drainage system where it intersects the Loon River valley, as well as secondary drainage patterns in the northeast corner of the Buffalo Head Hills. The highest concentration of northwest lineaments is traced in the southeast corner and eastern edge of the Buffalo Head Hills, where mapping is facilitated by high brightness contrast and texture variation.

The northeast-trending lineaments can be traced mainly in the northern portion of the Buffalo Head Hills and through the upper portion of the Loon River valley. The offset induced by the northeast lineaments is mainly observable along the Wabasca River in the eastern limit of the image.

The east-northeast–trending lineaments are regionally distributed from south to north and can be traced throughout the Buffalo Head Hills, the Loon River valley and part of the western limit of the Peerless Uplands.

3.4 RADARSAT-1 PC3 Structural Interpretation

The RADARSAT-1 PC3 image shows moderate tone variation and very clearly defined drainage patterns due to high contrast along drainage channels and the rich texture in the overall image (Figure 22).

The north-northeast linear trend is clearly defined and additional lineaments have been traced within the Loon River valley, the western boundary of the Peerless Uplands and in the central and southern portion of the Buffalo Head Hills (delineated by drainage patterns).

The northwest-trending lineaments in this image are mainly visible in the Peerless Uplands, along the Wabasca drainage and in the northeast corner and the central portion of the eastern edge of the Buffalo Head Hills. Northwest lineaments in the southeast corner of the image (Peerless Uplands) are recognized from texture and tone variations and occasionally topographic contrast; whereas along the eastern edge of the Buffalo Head Hills, they are outlined by texture and tone variation induced by the transition along the scarp from the Shaftesbury Formation and the overlying Smoky Group.

The northeast-trending lineaments are also very well defined in this image and confirm the distribution recognized in the RADARSAT-1 PC1 and PC2 images. Intersections between the northeast- and northwest-trending lineaments are well displayed along the Wabasca River in the eastern limit of the image.

The east-northeast–trending lineaments are also highly visible, due to strong textural and tone variations

and their apparent control on a few sections of the main drainage in the Wabasca River.

3.5 RADARSAT-1 PC4 Structural Interpretation

The RADARSAT-1 PC4 image is characterized by a diffuse pattern, which suggests increased noise, although some lineaments may still be recognized (Figure 23).

North-northeast–trending lineaments are detectable only in the northeast corner of the Buffalo Head Hills, plus a few in the northern portion of the Loon River valley and western boundary of the Peerless Uplands.

Northwest-trending lineaments are clearly visible in the western boundary of the Peerless Uplands due to good contrast and texture and tone variation, probably induced by lithological variation between the Shaftesbury Formation (medium grey) and the Smoky Group (light grey-white).

Northeast-trending lineaments are clearly defined in the central portion of the study area, the northeast corner of the Buffalo Head Hills and east of the Wabasca River. East of the Wabasca River, they are highlighted by high brightness contrast and texture and tone variation displayed within the Shaftesbury Formation.

East-northeast–trending lineaments are recognized in the image from variations in tone and texture. They are highlighted in a dark grey, east-northeast–trending corridor between the southeast corner of the Buffalo Head Hills and the Peerless Uplands.

4 Tectonic Framework

4.1 North-Northeast—Trending Lineaments

The north-northeast–trending lineaments have been previously identified in the Peerless Lake study (Eccles et al., 2000) and delimit, in particular, the inferred western margin of the north-trending Loon River graben (Figure 24). Their existence has been documented at surface as well to depth in the Precambrian basement; and they are interpreted to be associated with the propagation of the Peace River Arch structure. North-south–trending grabens have been documented in the central region of the Peace River Arch, which roughly parallels the underlying Ksituan-Chinchaga basement contact, and lie predominantly within rock of the Chinchaga Low (O'Connell et al., 1990). The northern margin of the Peace River Arch coincides with a north-northeast–trending lineament that is expressed in the underlying Precambrian basement surface (O'Connell et al., 1990). These observations suggest that the north-northeast–trending lineaments may originally have been Precambrian (O'Connell et al., 1990; Ross, 1990; Ross et al., 1991; Pilkington et al., 2000) and have influenced and/or partially controlled the development of the Peace River Arch structures during the Middle to Late Devonian. Moreover, magnetic data outline well defined fabric with a north-northeast–trending within the Buffalo High terrane and north-northwest- and north-northeast–trends within the Buffalo Utikuma terrane (Pilkington et al., 2000).

4.2 Northwest-Trending Lineaments

Northwest-trending lineaments were not recognized as surface features in the Peerless Lake study of Eccles et al. (2000), but were delineated in the Precambrian basement (Figure 25). Northwest lineaments

were also recorded in the Peace River Arch area in a combined study of the Precambrian basement surface and the Granite Wash (Devonian) isopach (Cant, 1988). Based on the thickness patterns of the Granite Wash, Cant (1988) suggested that these structures were normal faults with down-throw to the west-southwest. These kinematics are similar to the observed southwest down-throw of the southeast corner of the Buffalo Head Hills. The northwest-trending lineaments are attributed to the Middle to Late Devonian faulting phase of the Peace River Arch (Cant, 1988). More recently, Pilkington et al. (2000) outlined northwest-trending strike directions within the gravity data of the Buffalo High and Buffalo Utikuma terranes.

4.3 Northeast-Trending Lineaments

Northeast-trending lineaments have been documented as surface linear trends in the Peerless Lake study (Eccles et al., 2000), as well as in the Precambrian basement surface (Figure 26). Northeast-trending structures have previously been recorded in the basement and overlying sedimentary sequences of the Peace River Arch area (O'Connell et al., 1990). Here, the lineaments are parallel to the Arch axis and are, therefore, interpreted to be associated with its formation. The best known structure is the "Axial Graben," which is clearly defined in the uppermost Devonian Wabamun unit (Cant, 1988), and is also identifiable in the isopach map of the Delbot Formation of the Rundle Group (uppermost Mississippian). The northeast-trending lineaments were active during the Mississippian or block subsidence stage of the Peace River Arch (Cant, 1988). Northeast-trending lineaments have been documented on the exposed shield in Saskatchewan, under the thin sedimentary cover of eastern Alberta (Garland and Bower, 1959), and in the Precambrian basement at the eastern edge of the Peace River Arch (O'Connell et al., 1990). These observations suggest that the northeast lineaments may originally have been Precambrian in age and have been reactivated repeatedly during the Paleozoic (O'Connell et al., 1990).

A synthesis of electromagnetic studies in the Lithoprobe Alberta Basement Transect (Boerner et al., 2000) outlined the presence of conductive structures with inferred northeast strike direction bounding the Buffalo Head High terrane, and defined as the Kiskatinaw conductor, which may correlate with this northeast lineament set.

4.4 East-Northeast—Trending Lineaments

East-northeast–trending lineaments were not observed in the study of Eccles et al. (2000) (Figure 27). However, development of graben structures with dominantly east-west–oriented axes was documented in the northern edge of the western part of the Peace River Arch by O'Connell et al. (1990). Evidence for minor structures with roughly east-northeast–trends have been documented in the Peace River Arch within the lower Cretaceous sediments of the Bluesky Formation (Cant, 1988), perhaps related to the final subsidence of the PRA structures and the down-warp phase imposed by the evolving Laramide Orogeny. The east-northeast–trending features affect all the previous structures and Cretaceous sediments in the study area and, therefore, appear to be the latest tectonic event.

4.5 Discussion of the Outlined Structural Trends

The integration of the extracted lineaments for each identified dataset outlines well defined trends, with a strike variation from north to south throughout the study area; this is most clearly shown in the northwest- and northeast-trending lineaments highlighted in Figures 24 and 25. RADARSAT-1 PC2 offers the most effective image for structural interpretation in this area because it reveals all of the most

prominent linear features and clearly shows their correlation with topographic features and drainage patterns. This image is therefore used to display the data compilations.

From the compiled datasets, it is clear that the north-northeast and the east-northeast lineaments represent the most prominent linear trends in the area (Figures 23 and 26). The north-northeast–trending lineaments are probably controlled by Precambrian basement structures and, therefore, have been less affected or disrupted by the Peace River Arch development and related structures. On the other hand, the east-northeast–trending lineaments are the youngest of the outlined structural features and overprint all other evidence of tectonism in the area, and are possibly representing extensional fractures perpendicular to the northwest-trending compressional front imposed by the Laramide orogeny.

The northwest-trending lineaments seem to have the highest strike variability and separate the study area in two structural domains: the southern part, in which there is a general west-northwest–trending, and the northern part with a north-northwest–trending. This could imply variability and/or rotation of the stress field over time during the development of the northwest lineaments, or may reflect the presence of two distinct linear sets. This set of lineaments has been associated with originally Precambrian basement lineaments features (Cant, 1988; Pilkington et al., 2000) and has been reactivated repeatedly in the Middle to Late Devonian faulting phase of the Peace River Arch (Cant, 1988).

The northeast-trending lineaments also show strike variability from the southeast to the northwest corner of the study area. As for the northwest lineaments, two possible datasets can be extracted, which could reflect structural variability in the central and northern part of the Buffalo Head Hills study area. This angular variability is consistent with that observed in the northwest lineament dataset, and the two trends may form a conjugate set. This conjugate set of lineaments has been associated with original Precambrian lineaments that have been reactivated repeatedly during the Paleozoic (O'Connell et al., 1990). The northeast-trending lineaments are parallel to the Peace River Arch axis and have been active during the Mississippian or block subsidence stage of the Arch (Cant, 1988).

The results obtained in the structural analysis of the RADARSAT-1 PC imagery provide a level of detail of structural features that has not previously been seen using other optically-derived, remotely-sensed imagery. However, more work needs to be done in the analysis of the RADARSAT-1 PC imagery to understand better the physical link between the observed patterns and features observed in the field.

The validity of the structural analysis should be checked by using automated methods of feature extraction to eliminate potential errors induced by subjectivity of the interpreter. Furthermore, a statistical analysis of the extracted structural lineaments is needed to extrapolate general trends and to define structural domain variability. Such a refinement of the interpretation may better constrain the relationship between structural features and kimberlite emplacement in the study area.

Potential errors or uncertainties in the presented interpretations come from three main sources:

- method: slight discordance between the mapped interpretations of each RADARSAT-1 PC dataset is induced by the different geometric properties of each PC image
- subjective error may be introduced by the interpreter in recognizing and tracing linear features
- geological effects: angular variability may be related to tectonic effects of the latest events in offsetting or tilting earlier features

5 Preliminary Integration of RADARSAT-1 Principal Components, Digital Elevation Data, Geological Structure and Kimberlite Locations

Image integration consists of the fusion of multi-source remote sensing data to allow evaluation of complementary information, improvement of interpretation and increase in reliability of the outlined/interpreted patterns. The level of image fusion that has been applied in this preliminary study consists of the integration of RADARSAT-1 PC images and interpreted structural features, topographic surface digital elevation models (DEM), mapped geology and structural information and kimberlite locations.

5.1 RADARSAT-1 PC Colour Composite Imagery, Structural Data and Kimberlite Locations

Colour composite image integration assigns selected image bands (e.g., RADARSAT-1 PC) to the colours red, green and blue (RGB) to emphasize image features through chromatic contrast. Different combinations of RADARSAT-1 PC bands can be used to produce RGB colour composite images to facilitate pattern recognition (Grunsky, 2002).

One selected colour composite image of the Buffalo Head Hills area is shown as an example together with the extracted lineaments and kimberlite locations in Figure 28. Image enhancement using histogram equalization and Gaussian equalization has been applied to improve the colour balance and contrast of the colour composite images.

5.2 RADARSAT-1 PC123 (RGB)

In the image shown in Figure 28, the east-facing scarp of the eastern boundary of the Buffalo Head Hills is clearly outlined by a suite of north-northeast–trending lineaments. The RADARSAT-1 PC2 and PC3 images impart good textural contrast and topographic perception to the Buffalo Head Hills area, but highlight the Loon River valley not as well. The northwest- and northeast-trending lineaments are well outlined, as are some of the more prominent east-northeast trends in the southern portion of the Buffalo Head Hills and Peerless Uplands.

The structural interpretation of RADARSAT-1 PC2 is overlain on the image, and it can be observed that there is a good match between the major structural northwest- and northeast-trending lineaments and the green and purple colour variation. The same colour variation highlights the east-northeast–trending lineaments that cross the Loon River valley; this seems to correspond to areas with more sparse vegetation and high brightness values in the RADARSAT-1 PC1 and PC3 imagery. In the southern limit of the image, additional northwest-trending features can be delineated, which probably define structural scarps within the Shaftesbury Formation. The coloured visual enhancements of the east-northeast–trending lineaments across the Loon River valley and southeast corner of the Buffalo Head Hills enables a better definition of the intersection with the north-northeast–trending lineaments and reveals a possible spatial correlation with kimberlite occurrences.

5.3 RADARSAT-1 PC Colour Composite, DEM, Structural Data and Kimberlite Locations

A 100-m-resolution DEM of the land surface was used to emphasize the topography of the study area and provides a base on which the processed RADARSAT-1 PC colour composite images may be draped. For example, the draped RADARSAT-1 PC123 (RGB) image is shown in Figure 29. The interpretability of the colour composite image is much improved in this image, and the overlay of the extracted

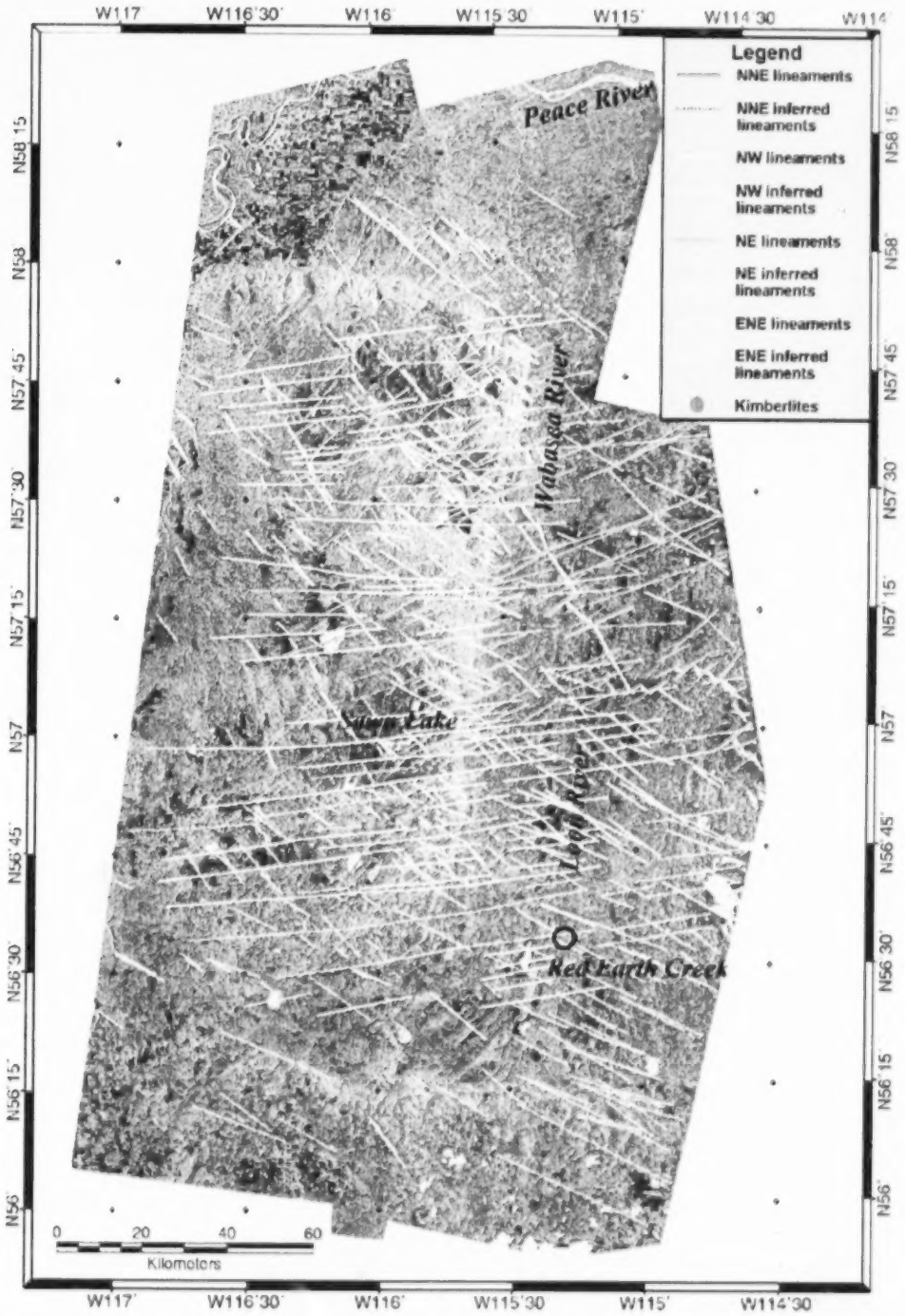

Figure 28. Colour composite Principal Components 1 (red), 2 (green) and 3 (blue) with structural trends and kimberlite locations.

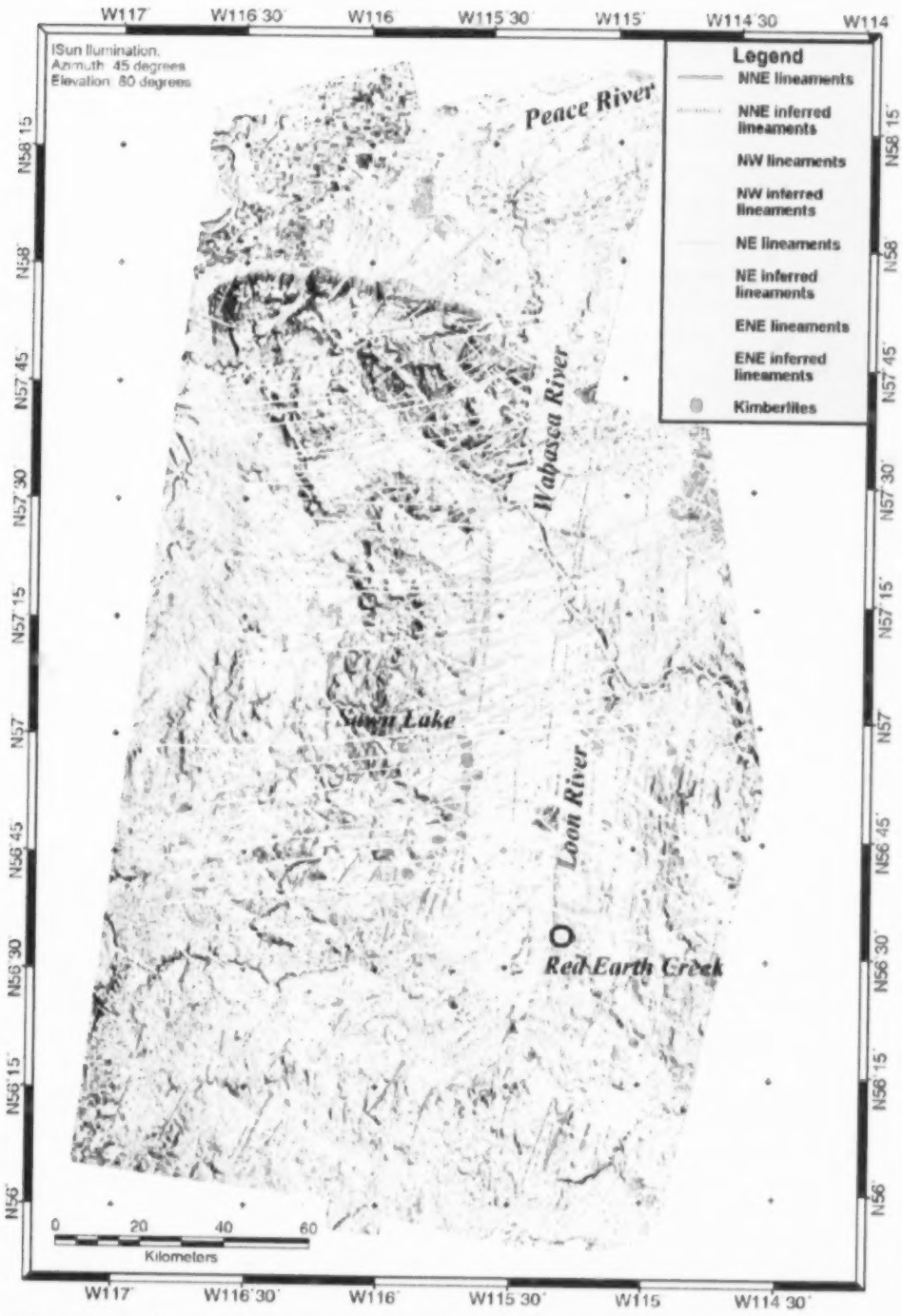

Figure 29. Colour composite of Principal Components 1 (red), 2 (green) and 3 (blue) draped on a Digital Elevation Model (DEM) with structural trends and kimberlite locations.

lineaments from RADARSAT-1 PC2 shows good correspondence to the highlighted topographic trends This implies that surface topographic information is preserved by principal components analysis of the original RADARSAT-1 data source and, therefore, supports its applicability for structural studies in this type of terrain.

This data integration technique emphasizes the probable structural control of the east-northeast lineaments on the topography of the southeast corner and southern boundary of the Buffalo Head Hills and southern portion of the image. Moreover, the topography appears to be strongly controlled by the northwest-trending lineaments in the northern part of the Buffalo Head Hills. In the southern part of the Buffalo Head Hills, the progressive strike variation of the northwest lineaments toward west-northwest trends is well outlined, and more linear features can be depicted in the southern part of the image, where they seem to define a topographic and probable structural escarpment. In the same portion of the image, the topography greatly emphasizes the presence of additional north-northeast–trending lineaments. This image further emphasizes the east-northeast–trending lineaments that cross the Loon River valley and the southeast corner of the Buffalo Head Hills, the spatial intersection with the north-northeast-trending lineaments and possible spatial correlations with the kimberlite occurrences.

5.4 RADARSAT-1 PC, Geology, Structural Data and Kimberlite Locations

The integration of the RADARSAT-1 PC with mapped geology enhances the visualization of textural variation due to surface roughness derived from changes in lithology and/or changes in vegetation as a response to lithology and soil characteristics. In Figure 30, the geology of the Buffalo Head Hills is draped on the RADARSAT-1 PC2 image and interpreted structural trends are overlain. The interpreted structures correlate with abrupt contact breaks in the lithologic sequence, this relationship being particularly well shown by northeast-trending lineaments in the northern part of the Buffalo Head Hills, in the central part by northwest-trending lineaments and in the eastern boundary of the Buffalo Head Hills and Peerless Uplands by north-northeast-trending lineaments. In Figure 30, known kimberlite locations are overlain on the geology and the structural trends. Some of the kimberlite locations show spatial correlation at the intersection of the outlined north-northeast–, east-northeast– and northeast-trending lineaments. Previous observation in the southeast corner of the Buffalo Head Hills have been made concerning the possible link and/or spatial correlation with north- and northeast-trending lineaments by Eccles et al. (2000). The presence of the youngest east-northeast lineaments, outlined in this study, may add a key element in the study of the factors that might have facilitated the emplacement of the kimberlites through the reactivation of the older north-northeast– and northeast-trending lineaments, which have been recognized from the literature and this study as arising from underlying basement structures.

6 Considerations for Further Work

Further refinement of the data integration techniques is likely to improve the structural interpretation of the Buffalo Head Hills area. Future work will use information derived from complementary data sources, such as Landsat7 TM data, Bouguer gravity and aeromagnetic surveys.

This work, and the future refinements using integrated Landsat7 TM and geophysical data, is intended to refine models for structural control of kimberlite emplacement in north central Alberta and hence aid further exploration in the area.

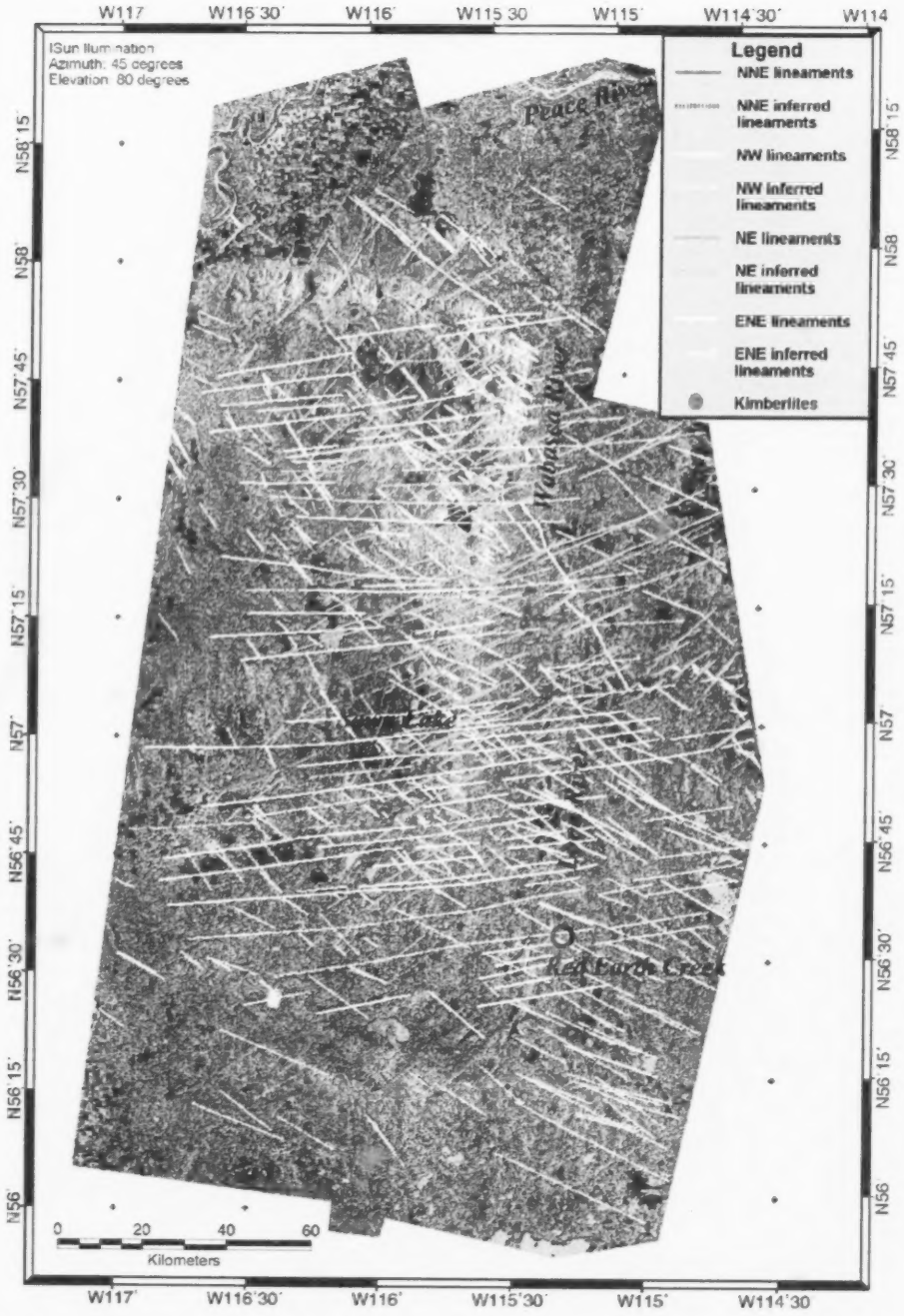

Figure 30. Geology of the Buffalo Head Hills draped on RADARSAT-1 PC2 with structuarl trends and kimberlite locations (red): Kl, Loon River Formation (Lower Cretaceous); Kp, Peace River Formation (Lower Cretaceous); Ksh, Shaftesbury Formation (Lower-Upper Cretaceous); Kd, Dunvegan Formation (Upper Cretaceous); Ks, Smoky Group (Upper Cretaceous).

7 References

Berger, Z. and Cartwright, R. (1997): Geological Exploration with RADARSAT, Exercise Manual. First International RADARSAT Conference, Calgary March 1997, 30 p.

Boerner, D.E., Kurtz, R.D., Craven, J.A., Ross, G.M., and Jones, F.W. (2000): A synthesis of electromagnetic studies in the Lithoprobe Alberta Basement Transect: constraints on Paleoproterozoic indentation tectonics. Canadian Journal of Earth Science, v. 37, p. 1509-1534.

Brown, R.J., Brisco, B., D'Iorio, M.A., Prevost, C., Ryerson, R.A., Singhroy, V. (1996): RADARSAT-1 applications: review of GlobeSAR Program. Canadian Journal of Remote Sensing, v. 22, n. 4, p. 404-419.

Cant, D.J. (1988): Regional structure and development of the Peace River Arch, Alberta: a Paleozoic failed-rift system? Bulletin of Canadian Petroleum Geology, v. 36, p. 284-295.

Carlson, S.M., Hillier, H.D., Hood, C.T., Pryde, R.P., and Skelton, D.N. (1998): The Buffalo Head Hills kimberlite province, north central Alberta, Canada. In: Seventh International Kimberlite Conference: Extended Abstracts. Cape Town, April 1998, p. 138-140.

Eccles, D.R., Grunsky, E.C., Grobe, M., and Weiss, J. (2002): Structural emplacement model for kimberlitic diatremes in northern Alberta. Alberta Energy and Utilities Board, EUB/AGS Earth Sciences Report 2000-01, 116 p.

Edwards, D.J., Lyatsky, H.V., and Brown, R.J. (1995): Basement fault control on Phanerozoic stratigraphy in the Western Canada Sedimentary Province; integration of potential-field and lithostratigraphic data. In: G.M. Ross Ed., Alberta Basement Transects Workshop, Lithoprobe Report 47, p. 181-224.

Evans, D.L., Farr, T.G., Ford, J.P., Thompson, T.W., Werner, C.L. (1986): Multipolarization Radar Images for geologic mapping and vegetation discrimination. *IEEE Transaction on* Geoscience and Remote Sensing, v. GE-24, n. 2, p. 246-257.

Garland, G.D. and Bower, M.E. (1959): Interpretation of aeromagnetic anomalies in the northeastern Alberta. Fifth World Petroleum Congress, Section 1-Paper 42, p. 787-800.

Grunsky, E.C. (2001): Mapping Geologic Structures and Surface Terrain over Large Regions using RADARSAT-1, http://orbit35i.nesdis.noaa.gov/orad/sarconference/Link_largescalemapping.with.radar.pdf

Grunsky, E.C. (2002): The use of multi-beam RADARSAT-1 imagery for mapping geologic structures and surface geomorphology. Alberta geological Survey Earth Science Report (in preparation).

Gupta, R.P., (1991): Remote Sensing Geology, Springer-Verlag, New York, 356 p.

Lewis, A.J., Henderson, F.M. and Holcomb, D.W. (1998): Radar Fundamentals: The Geoscience Perspective, in: Manual of Remote Sensing: Principles and Applications of Imaging Radar, 3rd edition Vol. 2, John Wiley & Sons, p 131-181.

Luscombe, A.P., Ferguson, I., Shepherd, N., Zimck, D.G., Naraine, P. (1993): The RADARSAT-1 synthetic aperture radar development. Canadian Journal of Remote Sensing, v. 19, n. 4, p. 298-310.

Mather, P.M. (1982): Computer Processing of Remotely-Sensed Images. John Wiley & Sons Publisher.

O'Connell, S.C., Dix, G.R., and Barclay, J.E. (1990): The origin, history and regional structural development of the Peace River Arch, Western Canada. Bulletin of Canadian Petroleum Geology, v. 38A, p. 4-24.

Paganelli, F. and Rivard, B. (2001): Contribution of the synergy of RADARSAT-1 and seismic imagery interpretation in the structural geology of the Central Alberta Foothills, Canada, as aid for oil and gas exploration. Canadian Journal of Remote Sensing, submitted.

Pilkington, M., Miles, W.f., Ross, G.M., and Roest, W.R. (2000): Potential-field signature of buried Precambrian basement in the Western Canada Sedimentary Basin. Canadian Journal of Earth Sciences, v. 37, p. 1453-1471.

Price, M.H. (1999): Integration of Landsat TM and SIR-C polarimetric radar for lithological mapping near Goldfield, Nevada. Proceeding of the Thirteenth International Conference on Applied Geologic Remote Sensing, Vancouver, British Columbia, March 1999, v. I, p. 452-4559.

Radarsat International, (1996): Radarsat Geology Handbook, <http://www.rsi.ca/resources/rghb.pdf>

Radarsat International, (1999): Radarsat User Guide, :<http://www.rsi.ca/resources/RSIUG98(499).pdf>, 113 p.

Ross, G.M. (1990): Deep crust and basement structure of the Peace River Arch: constraints on mechanism of formation. Bulletin of Canadian Petroleum Geology, v. 38A, p. 25-35.

Ross, G.M., Parrish, R.R., Villeneuve, M.E., and Browring, S.A. (1991): Geophysics and geochronology of crystalline basement of the Alberta Basin, western Canada. Canadian Journal of Earth Sciences, v. 28, p. 512-522.

Singhroy, V., and Saint-Jean, R., (1999): Effects of Relief on the Selection of RADARSAT-1 Incidence Angle for Geological Applications, Canadian Journal of Remote Sensing, Volume 25, No. 3, p. 211-217.

Singhroy, V., Slaney, R., Lowman, P., Arris, J., and Moon, W. (1993): RADARSAT-1 and radar geology in Canada. Canadian Journal of Remote Sensing, v. 19, n. 4, p. 338-351.

Smith S.K., Grieve, R.A.F., Harris, J.R. and Singhroy, V., (1999), The Utilization of RADARSAT-1 Imagery for the Characterization of Terrestrial Impact Landforms, Canadian Journal or Remote Sensing, Volume 25, No. 3, p. 218-228.

Appendix 1 – RADARSAT-1 Scene ID and Acquisition Date

RADARSAT-1 STANDARD MODE S1 ASCENDING

CC0014607	01 Oct. 1999
M0195960	08 Oct. 1999
M0195961	08 Oct. 1999
M0195962	08 Oct. 1999
M0196468	01 Oct. 1999
M0196470	01 Oct. 1999
M0198313	18 Oct. 1999
M0198314	18 Oct. 1999

RADARSAT-1 STANDARD MODE S1 DESCENDING

M0196088	09 Oct. 1999
M0196089	09 Oct. 1999
M0196090	09 Oct. 1999
M0196736	16 Oct. 1999
M0196737	16 Oct. 1999
M0196738	16 Oct. 1999
M0197302	23 Oct. 1999
M0197303	23 Oct. 1999

RADARSAT-1 STANDARD MODE S7 ASCENDING

M0197330	24 Oct. 1999
M0197331	24 Oct. 1999
M0197332	24 Oct. 1999
M0199941	24 Nov. 1999
M0199942	24 Nov. 1999
M0199943	24 Nov. 1999

RADARSAT-1 STANDARD MODE S7 DESCENDING

M0197356	24 Oct. 1999
M0197357	24 Oct. 1999
M0197358	24 Oct. 1999
M0199030	10 Nov. 1999
M0199031	10 Nov. 1999
M0199032	10 Nov. 1999

Appendix 2 – RADARSAT-1 Filtered Scenes

RADARSAT-1 STANDARD MODE S1 ASCENDING

CC0014607_GF
M0195960_GF
M0195961_GF
M0195962_GF
M0196468_GF
M0196470_GF
M0198313_GF
M0198314_GF

RADARSAT-1 STANDARD MODE S1 DESCENDING

M0196088_GF
M0196089_GF
M0196090_GF
M0196736_GF
M0196737_GF
M0196738_GF
M0197302_GF
M0197303_GF

RADARSAT-1 STANDARD MODE S7 ASCENDING

M0197330_GF
M0197331_GF
M0197332_GF
M0199941_GF
M0199942_GF
M0199943_GF

RADARSAT-1 STANDARD MODE S7 DESCENDING

M0197356_GF
M0197357_GF
M0197358_GF
M0199030_GF
M0199031_GF
M0199032_GF

Appendix 3 – RADARSAT-1 Mosaic Scenes

RADARSAT-1 STANDARD MODE S1 ASCENDING

MOSAIC_S1A

- CC0014607_GF
- M0195960_GF
- M0195961_GF
- M0195962_GF
- M0196468_GF
- M0196470_GF
- M0198313_GF
- M0198314_GF

RADARSAT-1 STANDARD MODE S1 DESCENDING

MOSAIC_S1D

- M0196088_GF
- M0196089_GF
- M0196090_GF
- M0196736_GF
- M0196737_GF
- M0196738_GF
- M0197302_GF
- M0197303_GF

RADARSAT-1 STANDARD MODE S7 ASCENDING

MOSAIC_S7A

- M0197330_GF
- M0197331_GF
- M0197332_GF
- M0199941_GF
- M0199942_GF
- M0199943_GF

RADARSAT-1 STANDARD MODE S7 DESCENDING

MOSAIC_S7D

- M0197356_GF
- M0197357_GF
- M0197358_GF
- M0199030_GF
- M0199031_GF
- M0199032_GF